STUDY OF WATER ABSORPTION BAND DEPTH FEATURES WITH VARIED SOIL PROPERTIES DURING THE DRYING PROCESS

A Thesis

Presented to the Faculty of the Graduate School

of Cornell University

In Partial Fulfillment of the Requirements for the Degree of

Master of Science

by

Jia Tian

February 2016

ABSTRACT

Selected spectral reflectance features of soils are examined with respect to their relationship to soil water content. Three soil samples selected to represent a range of particle size distribution, texture, and drying characteristics were monitored as the samples progressed from fully saturated to air dry. Spectral reflectance was collected over the wavelength range 350 nm to 2500 nm, a range in which four major water absorption bands exist: two in the visible/near-infrared (VNIR) region centered at 970 nm and 1160 nm, and the other two in the shortwave infrared (SWIR) region centered at 1440 nm and 1930 nm. The water absorption bands were the focus of this work with the expectation that these features would be the most sensitive indicators of the surface water content. However, the two absorption features in VNIR region were not useful for all three soils, so the two absorption bands in SWIR region became the focus in this study, especially the more sensitive 1930 nm band. Plots of the changing absorption band depths in the SWIR region were similar in shape among three soil samples. Three to four approximately linear stages were observed over the whole drying process, however, the transitions between drying stages did not occur at consistent points in the drying process, making it difficult to build a direct relationship between the absorption features and volumetric water content that would be independent of the soil type.

Although no general, soil-independent relationship could be found between an absorption feature and volumetric water content, there were characteristic changes in the band depth features that were coincident with evaporation stage transitions. Initially, the depth of the band centered at 1930 nm increased steadily and slowly with decreasing soil water content, reached a maximum, and then abruptly decreased marking a distinct change between the early and late,

relatively steady drying rate stages. During the late stage, the magnitude of the band depth decreased sharply with only a small change in water content. The decrease was coincident with the water evaporation transition from stage-1 (constant, relatively fast evaporation rate) to stage-2 (slower evaporation rate), a transition which is related to the exhaustion of pore water and the initial loss of adsorbed water.

The two SWIR water absorption band depths did not decrease with decreasing soil water content monotonically, which is counterintuitive. In order to understand the process, a simple mathematical model was built which suggested that the pattern of change in the band depth was related to the near extinction of light at the band center relative to the band shoulders. This extinction can be related to a specific water optical path length. The maximum absorption band depth at 1930 nm (and the associated water optical path length) appears to coincide with a trace amount of water present in the pore spaces for all three soil samples, which is consistent with the transition in drying rates.

BIOGRAPHICAL SKETCH

Jia Tian was born in a scholar family in Beijing, China. When Jia was in Beijing, her mother and grandparents gave her great influence on arts, especially on Chinese classical literature. Their acquaintance on literatures made Jia admire people who are experts in some domain and want to be a professor like them.

In her early teens, she moved to Nanjing with her parents. Nanjing was the capital city of six dynasties and is a city full of profound historical culture. The cultural atmosphere in Nanjing kept confirming Jia's inspiration on academic field. During that time, she found herself more talented in logical reasoning disciplines than arts and literature. As a result, she decided to focus on science and engineering as her father.

In 2008, Jia Tian was enrolled in School of Electronic Science and Engineering, Nanjing University, and was conferred bachelor degree of science four years later. In Nanjing University, she learnt how to focus on research and solve problems. Meanwhile, she felt that she was more attracted by disciplines related to nature. From her father's advice, she knew remote sensing, and was attracted by the combination of field experiments and laboratory processing.

Motivated by her interest and a good chance, Jia continued her M.S./Ph.D. study in Cornell University majoring in Remote Sensing. Working with Professor William Philpot, Jia focused on soil water content research using hyperspectral methods.

谨以此献给我爱的家人。

This work is dedicated to my beloved family.

ACKNOWLEDGMENTS

I would like to thank my advisor, Professor William Philpot, for giving me unconditional support on my study. He introduced remote sensing to me, and guided me to scientific research. He showed me the charm of science as well as the dedication of a researcher, and his effort gave me an unforgettable impression on insistence and earnestness.

I would like to thank my committee members, Professor Murray McBride and Professor Harry Stewart, who expanded my view. I learnt many related knowledge, which will help me in my further study. They let me know the relationship among different disciplines and gave me the potential to solve problems from different aspects.

I would like to thank my friends Shule, Peipei, Jiajun, Haoran, Yilin at Cornell for helping each other and making my life colorful. I would like to thank the wonderful friends I met at Cornell and in Ithaca throughout my graduate school career, there are too many to list.

Most importantly, I am grateful to my family. My parents and grandparents let me make my own choice, pursue my ideal, and have faith in me. They support me to study aboard, though this means we will be apart at some important moments in several years. My father, Qingjiu Tian, shows me hard working; my mother, Wei Yang is always considerate to me. All the good personality I had is learnt from them, and they still help me be a better person. Finally, I want to thank Xiaodong Wang, for always being there with me whenever I met difficulties.

TABLE OF CONTENTS

ABSTRACT II

BIOGRAPHICAL SKETCH iv

DEDICATION v

ACKNOWLEDGEMENT vi

1. INTRODUCTION 1

2. LITERATURE REVIEW 4

2.1 SOIL MOISTURE CONTENT IN AGRONOMY 4

2.2 GROUND MEASUREMENTS 5

2.3 SURFACE SOIL MOISTURE – ROOT-ZONE ZONE SOIL MOISTURE 6

2.4 MICROWAVE REMOTE SENSING 6

2.5 EVAPORATION 7

2.6 SOIL CLASSIFICATION 8

2.7 OPTICAL REMOTE SENSING: REFLECTANCE IN THE SOLAR DOMAIN 8

3. EXPERIMENTAL DESIGN 11

3.1 SOIL SAMPLES 12

3.2 EQUIPMENT 13

3.2.1 SAMPLE HOLDER 13

3.2.2 SCALE 14

3.2.3 SPECTROMETER AND LAMP 14

3.2.4 MICROMETER 15

3.2.5 MICROSCOPE 15

3.3 EXPERIMENTAL SETUP 17

3.4 EXPERIMENTAL PROCEDURE 17

4. METHODOLOGY 20

4.1 DEPTH OF WATER ABSORPTION BANDS 20

4.2 VOLUMETRIC WATER CONTENT 23

4.3 SAMPLE DEPTH 23

5. RESULTS 26

5.1 BAND DEPTH SEGMENTATION 30

5.1.1 QUARTZ SAND 30

5.1.2 MASONRY SAND 33

5.1.3 ITHACA SOIL 35

5.2 BAND DEPTH AND VWC 39

5.3 RATE OF CHANGE IN BAND DEPTH AND EVAPORATION 45

5.4 A SIMPLE MODEL 50

6. CONCLUSION 55

7. REFERENCE 59

1. Introduction

Soil moisture content is a key factor for many fields of study, such as hydrology, meteorology and agronomy. For example, in agronomy, moisture content distribution is important for crop growth monitoring and agricultural production prediction. In hydrology, soil moisture is indispensable for the study of the movement, distribution, and quality of water on Earth. In particular, the surface soil moisture content is not only an indicator for deeper water content, but is also essential for ground-atmosphere energy exchanges.

Conventionally, several geophysical methods are used for in situ measurements of soil moisture (Parent et al. 2006; Gaskin & Miller 1996; Ozcep et al. 2009). These methods are easily calibrated and allow detection of soil moisture content at the root-zone depth, which is important for agricultural crops. While these measurements are effective for the detection of water content at depth, they are typically time consuming and costly, making it difficult to collect dense observations over large areas or to monitor changes over time. In contrast, remote sensing and proximal sensing techniques acquire information without making physical contact. Remote sensing systems on satellite or aircraft have the potential for obtaining data over a large area at high spatial resolution. Proximal sensing systems have the potential for providing rapid in-field measurements and for monitoring change over time.

The most common remote sensing methods for observing soil water content use passive microwave radiation, taking advantage of the capacity of microwaves to penetrate through damp soil at microwave wavelengths. Unfortunately, the capacity to penetrate the soil means that the

measurements are integrated over the depth of penetration, with no information specific to the water content of surface and near-surface soil.

Optical remote sensing is another approach to detecting the surface soil moisture content. The presence of moisture greatly influences spectral reflectance in both the visible/near infrared (VNIR: 400-1200 nm) and the shortwave infrared (SWIR: 1200-2500 nm), especially in the major water absorption bands centered at 970 nm, 1160 nm, 1440 nm, and 1930 nm. It is reasonable to expect that the water absorption features would be very sensitive to the surface soil water content, and the depth of these water absorption features is hypothesized as an effective parameter for monitoring and describing the whole drying process. Water absorption features are not generally considered for remote sensing applications because the strong atmospheric absorption by water vapor in the vicinity of these bands leads to very low signal-to-noise values. Indeed, remote sensing systems are generally designed to avoid these wavelength regions. However, for proximal sensing where the illumination is supplied locally, the water absorption bands are prominent in the reflectance spectra, making it worthwhile to study the relationship between depth of water absorption bands and surface soil moisture content.

A useful optical measure of soil moisture would be sensitive to the soil water content from saturated to dry conditions, and would be applicable to any type of soil. The initial hypothesis was that, the depth of water absorption bands meets these two requirements. This study was designed to explore that hypothesis and to develop a model derived from the depth of the water absorption band to estimate soil water content with optical remote/proximal sensing. In addition, in order to consider the effect of evaporation on continuous reflectance change, the whole drying process was observed in this study.

The goals of this thesis are to:

1. Describe the pattern of change in the depth of the major water absorption bands during the whole drying process, and determine if the pattern is consistent among soils with different physical and chemical properties;
2. Find an empirical, mathematical model relating soil water content and absorption band depth that fits the observations.
3. Examine the relationship between the optical measure of spectral features and the evaporation rate.
4. Build a theoretical model to explain the mechanism of changing spectra in soil samples during the drying process.

2. Literature Review

Soil moisture has been studied for many decades because it is a key factor for many fields of study, such as hydrology, meteorology and agronomy (Wigneron et al. 1998). For applications in which moisture at or near the surface is important (e.g., agronomy), there are a variety of techniques that have been developed to measure soil moisture including both probe-based ground measurements and remote sensing methods. The ground-based methods are the proven, reference observations, but remote sensing techniques hold promise for providing more extensive aerial and temporal observations. This section provides a brief review of the current surface soil moisture measurement techniques, with emphasis on agronomic applications.

2.1 Soil moisture content in agronomy

The potential rooting depth of most agricultural crops ranges from about 0.6 to 1.5 m, and the maximum rooting depth is normally less than the potential rooting depth due to physical and chemical barriers. The distribution of water extracted by plants from soil varies with depth (Figure 2.1) with more water being extracted from shallower depths (Evans, 1996). To study the influence of soil water content on crops, measurements of soil water should extend down to a significant portion of the root zone depth. Given the depth of the root zone and the effective penetration depth of different techniques, the most appropriate methods are ground-based measurements and microwave remote sensing. However, optical measurements have a place in the overall measurement scheme and, as will be discussed below, have some unique advantages.

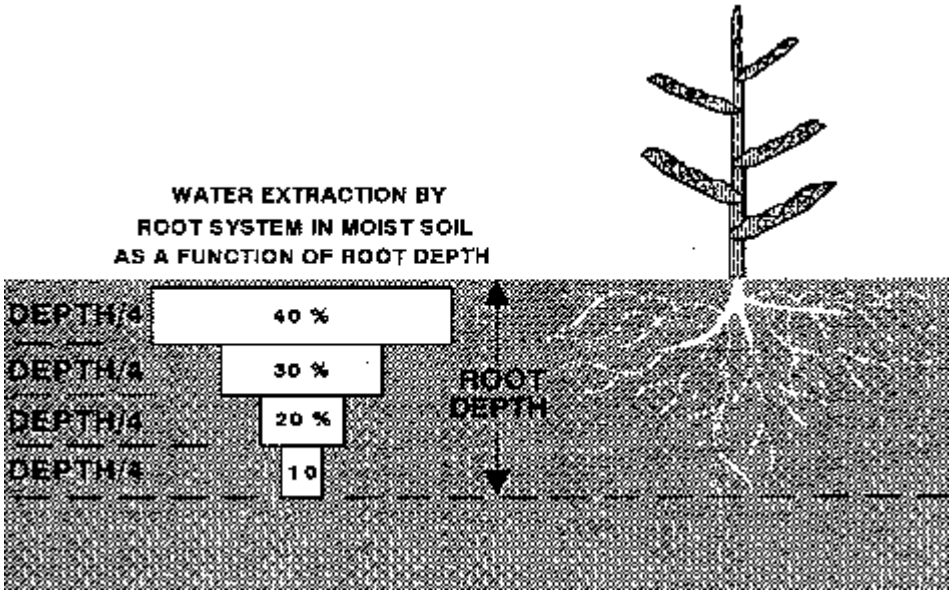

Figure 2.1: The amount of water extracted by plants is influenced by the distribution of the root in the soil (Evans, 1996).

2.2 Ground Measurements

There are many ground-based techniques for measuring soil moisture in the field, including time-domain reflectometry (Parent et al. 2006), frequency domain sensors (Gaskin & Miller 1996), electrical resistivity tomography (Ozcep et al. 2009), and ground penetrating radar. Most of these methods are effective with larger soil volumes and are not as useful for characterizing moisture in the upper few centimeters (Zhu et al. 2010).

Ground measurements usually provide data that are easily calibrated, but each measurement only applies to a single, small area. They are easily adapted to monitoring temporal variations (Parent et al. 2006), but are difficult to use to map spatial variations. The most prominent advantage of the ground-based measurements is in providing soil moisture content at root-zone depth, the most appropriate range for agricultural studies.

2.3 Surface soil moisture – root-zone zone soil moisture

Soil moisture content, as studied in agriculture, is normally required over large areas. However, the difficulty and expense of ground measurements makes it problematic to collect measurements at multiple sites or even to make frequent observations at a single location. Because of the inconvenience of direct root-zone soil moisture measurements, other, more easily-obtained parameters are often used for moisture estimates. For example, Mahfouf (1991), reasoning that near-surface temperature and humidity are influenced by the soil moisture, developed a model to describe the effect, and then, inverting the model, used the above-surface measurements of temperature and humidity to retrieve the soil moisture in root-zone as verified using in-ground methods: neutron sounding (soil-water profile) and gypsum blocks (first 5 cm of the soil). Although the results showed promise, the link between air temperature/humidity and root-zone soil moisture is rather indirect and imprecise.

2.4 Microwave remote sensing

Microwave remote sensing systems may be either active or passive. Active (radar) systems transmit an electromagnetic pulse and measure the energy scattered back, while passive radiometers observe the energy emitted from the target itself (Ulaby et al., 1982). Microwave remote sensing has the general advantage of being unaffected by cloud cover and not requiring solar illumination. This all-weather capability is particularly true for systems that operate in the low frequency microwave range (1 – 10 GHz) (Njoku & Rague 1996; Wagner et al. 2006).

For a number of years, microwave remote sensing methods have been the main focus of research aimed at retrieving the moisture content of the top several centimeters of soil (Walker et al. 2001; Sabater et al. 2007; Albergel et al. 2008; Ford et al. 2014). Sabater et al. (2006) also studied four data processing methods. The overall result of their study indicates that all four

methods yield satisfactory results, which suggests that retrieving root-zone soil moisture content from surface soil water content is feasible.

Soil moisture content most strongly affects passive microwave radiation from soils due to the difference between the dielectric constant of water (~80 at frequencies below 5GHz) and that of dry soil (~3.5) (Njoku & Entekhabi 1996); the soil dielectric constant increases with increasing water content. However, the measurement of radiation is also influenced by soil surface roughness (Choudhury et al. 1979; Tsang & Newton 1982; Mo et al. 1987), attenuation and emission by vegetation cover (Jackson 1982; Pampaloni & Paloscia 1986; Jackson & Schmugge 1991), and surface and subsurface heterogeneity (Tsang et al. 1975; Wilheit 1978; Kerr & Njoku 1990). The most recent global soil moisture measurement is provided by the Soil Moisture Active Passive (SMAP) satellite mission. SMAP was launched on January 31, 2015, and one of its objectives is to measure the amount of water in the top 5 cm of soil of the Earth. Compared to optical remote sensing, SMAP is able to estimate deeper soil moisture content by integration every 2 to 3 days. However, microwave systems like SMAP can only provide data on the landscape scale (kilometers to 10s of kilometers). They are incapable of finer, field-level observations. Microwave systems are also not readily adaptable to ground observations or for monitoring evaporation.

2.5 Evaporation

Evaporation is a key hydrologic driver that directly connects surface soil moisture content to the atmospheric water vapor content. Direct soil evaporation and plant transpiration consume 20% and 40% of the water introduced water by terrestrial precipitation, respectively (Oki & Kanae 2006; Or et al. 2013). Sherwood (1929) pointed out that, at the beginning of the drying process, very wet solids exhibit a period with a constant rate of drying which only decreases

once the soil reaches a critical liquid content. These two periods are called the constant rate period and the falling rate period. The constant rate period is supported by internal capillary flow (Van Brakel & Heertjes 1978; Yiotis et al. 2006), with water in the near-surface moving to surface so that the rate of drying remains constant. During the falling rate period, the available pore water is exhausted, and the evaporation rate is then limited by the vapor diffusion path and is no longer supported by capillary flow. When water loss is due to evaporation, the change in evaporation rate is related to the loss of available pore water.

2.6 Soil classification

Because the type of soil influences the evaporative process (Lehmann & Or 2009), soil classification is one of the essential issues facing remote sensing observations. In some cases the classification can be based on characteristic spectral features, as with Lesaignoux et al. (2010) who sorted soil samples into organic matter-rich, lime-rich, and iron oxide-rich groups. For in situ work, samples can be labeled by soil order in the USDA soil taxonomy (USDA, 1999). In other studies, soil samples might be described by their different material content (Liu et al. 2002), or color (Lesaignoux et al. 2013).

2.7 Optical remote sensing: reflectance in the solar domain

A distinct problem with drawing a relationship between soil moisture (as defined for agricultural or hydrological purposes) and optical sensing is that optical radiation does not penetrate soil beyond the surface layer; the reflectance derives only from the first several millimeters of soil at most (Liang 1997). We will refer to this depth as the “optical surface”. There is a demonstrable link between the soil optical surface and root zone soil moisture, as there are many studies that have drawn a connection between volumetric soil moisture (as determined

by weight) and the reflection from soil surfaces in the visible/near infrared (VNIR) and the shortwave infrared (SWIR) spectral regions (Kaleita et al. 2005; Ahmad et al. 2011).

To study the relationship between soil reflectance in the optical domain (400 - 2500 nm) and soil moisture, several wavebands are usually selected by some form of optimization method, and then used to indicate reflectance changes for a particular set of soil samples. Typically, a linear forward stepwise regression technique will be used for the optimization. For example, Liu et al. (2001) determined an optimal band set that included 1400, 986, 1998, 574, 2189, 1672, and 450 nm, listed in the order of importance. In another study (Lobell & Asner 2002), a single wavelength, 2200 nm, was selected based on its absorption response in mineral soils, and 600 nm and 1200 nm were included for contrast. Different studies also take a variety of approaches to calibration and normalization. For example, Lobell and Asner's (2002) results were based on absolute reflectance, while Liu (2001) focused on normalized reflectance, i.e., dividing the reflectance from a wet soil by the reflectance of the same type of soil when it was dry. This minimizes variations due to roughness and sensor-source geometry effects (Baret et al. 1993). Among these studies, researchers were trying to find an effective way to extract spectral features from reflectance to explore the relationship to soil water content. However, there is still no unified way to represent reflectance features; researchers continue to introduce new parameters that are appropriate for their studies.

To estimate the soil moisture content from reflectance in the optical domain, researchers usually rely on empirical rather than on physically-based models. A typical approach is to employ an exponential model describing the relationship between reflectance and soil moisture content (Lobell & Asner 2002; Zhu et al. 2010), but a combination of linear and nonlinear functions has also been proposed, as has an empirical model that relies on a polynomial

relationship (Lesaignoux et al. 2010). In Bach and Mauser's (1994) research, two processes are taken into account. One is the general darkening of soil due to internal reflection in a surface water layer and the other one is absorption by water contained in soilat certain wavelengths.

All of these studies focus on reflectance values, and most showed reflectance consistently decreasing with increasing soil moisture content (Planet 1970; Stoner & Baumgardner 1981; Choudhury et al. 1979; Chang et al. 2005; Lesaignoux et al. 2013). There are a few studies, however, that have indicated that reflectance can increase at higher soil moisture content after a certain level of water content (Neema et al. 1987; Liu et al. 2002), and the level was different for different types of soil (Liu et al, 2002). There is some indication that the inversion may be caused by specular reflectance from a water film covering the soil surface due to oversaturation (Sadeghi et al. 2015). In Sadeghi's research, a physically-based soil moisture retrieval model was developed to estimate reflectance as a function of soil water content over the full optical domain (350 nm – 2500 nm). Most of the existing research results indicate that the SWIR region is more suitable than the VNIR for mapping the relationship between spectral reflectance from the soil surface and soil moisture content (Lobell & Asner 2002; Zhu et al. 2010). As Lobell and Asner (2002) indicated with their empirical model, reflectance in the SWIR region is responsive to a wider range of soil moisture, up to 50% volumetric water content, while the reflectance in the VNIR region can reach a minimum when the soil moisture content is on the order of 20%. Secondly, the uncertainly in the estimate of soil moisture content based on SWIR observations was only half the uncertainty for similar estimates based on observations in the VNIR region. However, Liu et al. (2002) points out that the shorter wavebands could provide a more reliable estimate at high moisture levels.

All the existing work focuses on differences in soil reflectance for several discrete levels of water content, and does not consider the continuous change in the reflectance with moisture content. In addition, most of the existing work uses simple, empirical models to describe the correlation between water content and reflectance using a few optimally selected spectral bands. In contrast, the research presented here addresses the change of reflectance with evaporative loss using the depth of water absorption bands, a spectral feature directly influenced by water content. As a result, this study was designed to build a relationship between water absorption band depth and soil water content that would be independent of soil type. If successful, the relation could be used for all types of soils without the need for soil classification.

3. Experimental Design

To design a series of experiments to achieve expected data, two main aspects are considered. First, the soil samples should be varied in physical and chemical characteristics, which will help in building a more general model relating soil water content and a spectral feature. Second, the experiment should be designed to collect spectral reflectance and soil sample weight data continuously to describe the whole drying process. The selected soil samples, equipment, experimental setup and procedure will be illustrated in this section.

3.1 Soil samples

Soil reflectance varies with the type of soil, the particle size distribution and the bulk density of the soil, in addition to the water content. To obtain a set of reflectance measurements that would be representative of the range in possible changes during the drying process, three samples (Table 3.1) were observed in the experiments. They are varied in color, degree of transparency, density, particle size, and composition.

1. Quartz sand: The sand sample consisted of white, relatively translucent, 90% silica particles. The sand particles were quite homogeneous in size with an average diameter of about 1 mm. Because of the white color, translucence and low absorption, the spectral reflectance is high relative to most soils.
2. Masonry (dark) sand: The sand sample is generally light brown with some black particles. The particle size is not as homogeneous as the white sand, but it is finer with an approximate average diameter of 50 microns. The reflectance of dark sand is lower at all wavelengths than white sand.

3. Ithaca soil: This is the only natural soil among the three samples. It is from a local orchard, and has a relatively high content of clay and organic matter. The original sample was not homogeneous in particle size, but contained a number of larger particles: pieces of plants' roots, or aggregates of fine particles. For the experiment, the large particles were removed.

Table 3.1: Soil physical characteristics

	quartz sand	masonry sand	Ithaca soil
Very coarse and coarse sand	86.1%	18.3%	3.8%
Medium sand	10.1%	27.0%	
Fine and very fine sand	3.8%	48.4%	
Silt	0%	4.4%	77.0%
Clay	0%	1.9%	19.2%
Texture*	Coarse sand	Sand	Silty loam
Bulk density	1.44 g cm^{-3}	1.53 g cm^{-3}	0.95 g cm^{-3}

* Texture classification is based on USDA standard.

3.2 Equipment

3.2.1 Sample holder

The sample holder was a 1.2 cm tall, gray, plastic cylinder with a 5.1 cm inner diameter and a screen glued to the bottom. The total volume of the sample holder was

$$V_{total} = \pi r^2 \cdot h, \quad (3.1)$$

where V_{total} is the available volume, r is the radius, and h is the height of sample holder. The volume of the sample holder was then 24.5 cm^3. The sieve bottom allowed water to be drawn up

into the sample by capillary action, minimizing disturbance of the soil surface and also minimizing the opportunity for air to occupy the pore spaces.

Figure 3.1: Sample holder with screen bottom.

Figure 3.2: Ohaus scale

3.2.2 Scale

An Ohaus SP200 scale (Figure 3.2), with a 0-2000 g range and a precision of 0.1 g was used to monitor the weight of the sample during the experiment. Black tape was used to cover the surface of the balance to reduce the possibility of reflected light from the balance reaching the spectrometer input optic. The balance was linked to a computer via a USB connection, providing continuous monitoring without the need to move the sample.

3.2.3 Spectrometer and Lamp

The spectrometer was an ASD FieldSpec® Pro (Figure 3.3) with a spectral range of 350-2500 nm, and a resolution of 1 nm. Illumination was provided by an ASD Pro Lamp (Figure 3.4)

which is designed to provide stable, DC illumination over the full spectral range viewed by the ASD spectrometer.

Figure 3.3: ASD spectrometer

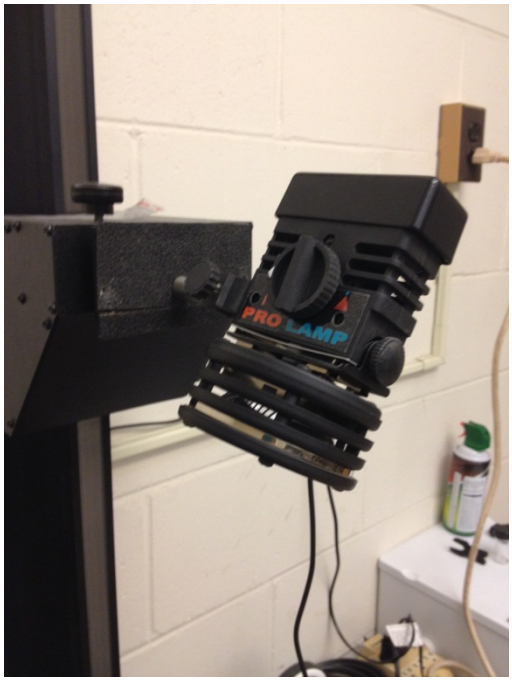

Figure 3.4: Lamp

3.2.4 Micrometer

A Westward micrometer (Figure 3.5), with a range of 0-27 mm and an accuracy of two digits after the decimal point was used to measure the depth of the sample.

3.2.5 Microscope

A Celestron® handheld Digital Microscope PRO (Figure 3.6) was used to image the soil surface throughout the experiment. The original plastic base was not sufficiently stable and was replaced with a solid aluminum base. Eight LED bulbs surround the optical port of the microscope and illuminate the viewing area. Black tape was applied to the clear plastic shield surrounding the LED and input optics to block the IR-rich light from the ASD Pro lamp and to

prevent the LED radiation from illuminating the field of view (FOV) of the spectrometer. The microscope was connected to the computer through a USB connection, and images were collected under program control.

Figure 3.5: Micrometer

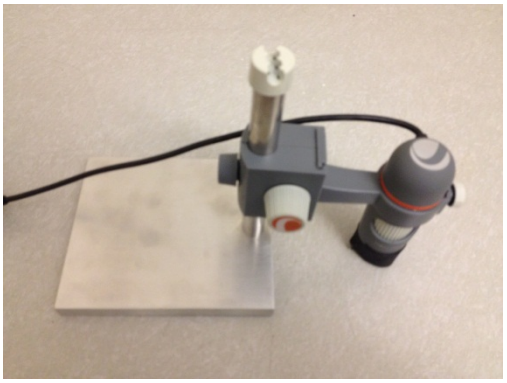

Figure 3.6: Microscope

3.3 Experimental Setup

The ASD probe was fitted with an 8 degree field of view (FOV) foreoptic and mounted 18 cm above the soil sample (nadir view). The diameter of the FOV on the soil sample was then 4.2 cm. The lamp was set at a 30 degree zenith angle, at a height of 50 cm above the sample and a horizontal distance between sample center and lamp of 30 cm, providing a roughly uniform illumination over the detector viewing area on the sample (Figure 3.7).

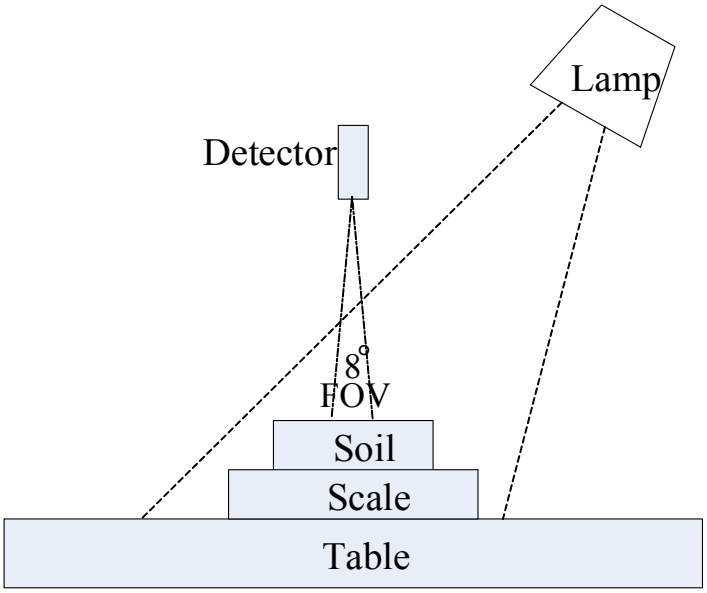

Figure 3.7: Equipment setup

3.4 Experimental Procedure

The overall experimental procedure is diagramed in Figure 3.8. In the preparation stage, prior to the full experiment, each soil sample was tested to ensure that the 1 cm depth of the sample holder would be deep enough to avoid reflectance from the bottom of the sample holder. The approach of measuring the depth of penetration will be illustrated in Section 4.3.

For the main experiment the intent was to observe the change in reflectance for each sample due only to the change in water content; the setup and procedures were designed to minimize any other factors. To this end, water was introduced by infiltration through the screen at the bottom of the sample holder and wetted the sample via capillary action. This minimized any possibility of disturbing the prepared soil surface and also reduced the chance that air would be entrained in the pore spaces. Data collection was automated, with spectral reflectance of the sample being monitored at 10 minute intervals. Sample weight was recorded at one-minute intervals but is reported in 10-minute intervals, averaged over 10 minutes. Images of the soil surface during the drying process were also collected at 10-minute intervals.

After the data collection, spectral data were processed: calibrated reflectance was computed, band depth parameters were derived from the spectra, and volume water content (VWC) was computed and linked to the spectral reflectance observations.

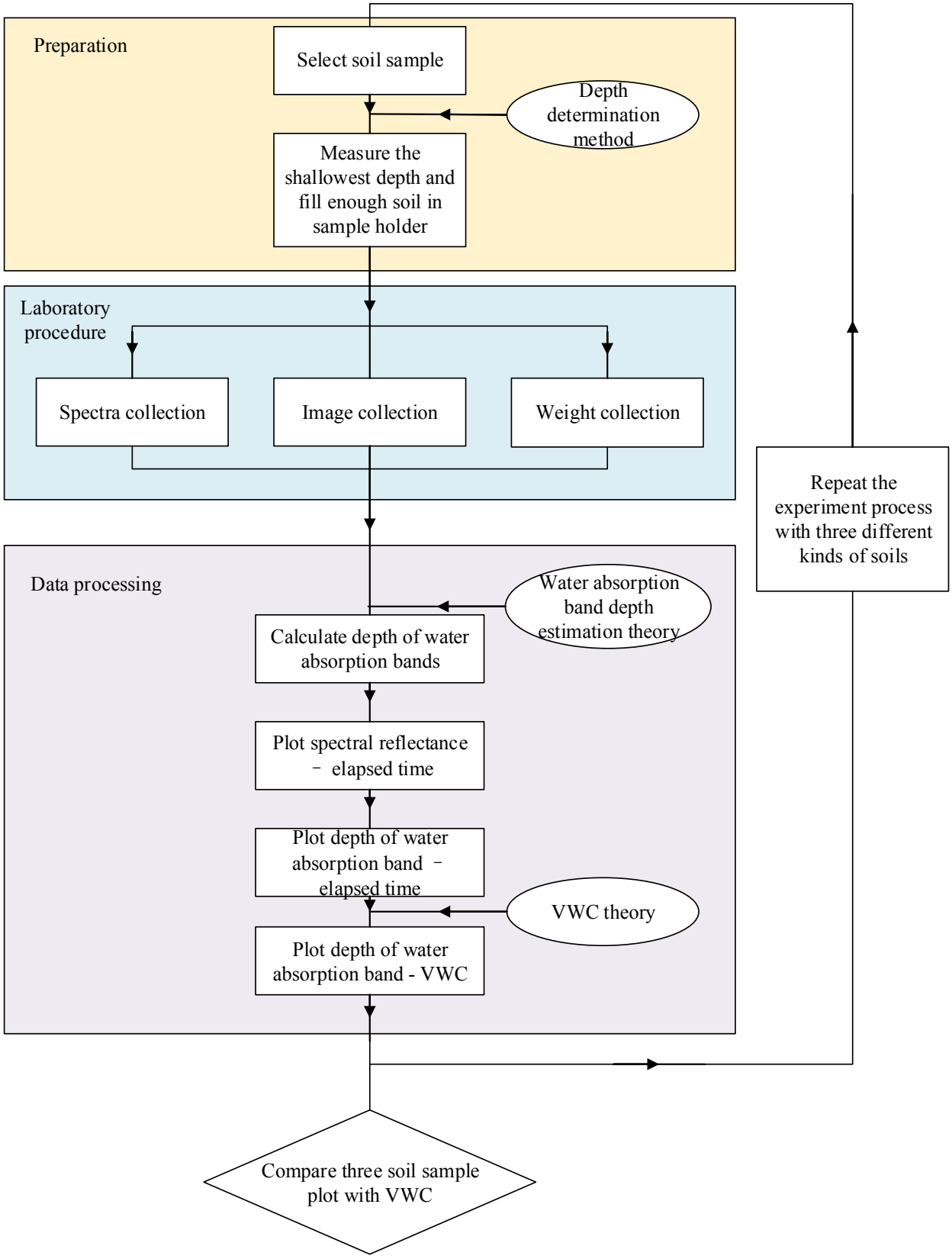

Figure 3.8: Experimental setup

4. Methodology

In this study, the relationship between soil water content and reflectance was the critical measurement, and it was particularly important that the metrics be appropriate and comparable to each other over different soil types. Based on this requirement, the depth of the water absorption bands and the VWC were selected to characterize the reflectance and soil water content, respectively. In this section, the methods of calculating the water absorption band depth and VWC were described.

In addition, since the sample depth used for the experiments was relatively shallow (1.2 cm) it was important to confirm that the soil sample was optically deep, i.e., that none of the detected light had interacted with the bottom of the sample holder. The shallow depth was designed to minimize the amount of time required for drying, but the sample depth had to be sufficient to ensure that the reflectance spectra were characteristic only of the damp soil, not the sample holder. The procedure used to confirm the adequacy of the sample depth is also described in this section.

4.1 Depth of water absorption bands

Water is relatively transparent in the visible, but becomes increasingly absorptive beginning in the red and increasing throughout the infrared. In addition to this broad absorption, there are strong water absorption bands due to the vibration of hydroxyl ions in water, and the depth of these water absorption features is a sensitive indicator of the soil moisture content.

In hyperspectral remote sensing, the depth of an absorption band of a target material is commonly used as an indicator of the amount of that material present within a host material. When absorption by the target material is negligible away from the center of the absorption band,

a normalized absorption band depth is recommended to minimize the effect of the differences in reflectance of different host materials (Clark & Roush 1984). With water, however, absorption is strong throughout the infrared and is extreme in the SWIR. Absorption at these wavelengths by the host material (soil) is negligible; the band depth registers the spectral difference in attenuation of water at the band center and the band shoulders. For wet soil, then, a simple difference measure of the band depth is appropriate, and likely provides more consistent information than either simple reflectance or a normalized band depth. A simple estimation of band depth is given by the vertical distance from the minimum reflectance to a straight line connecting the shoulders of the water absorption feature. The interpolated reflectance, R_{int} , on the connecting line at the center wavelength is given by:

$$R_{int} = \frac{R_{left} - R_{right}}{\lambda_{left} - \lambda_{right}} * \left(\lambda_{center} - \lambda_{left}\right) + R_{left} \quad , \tag{4.1}$$

The band depth, ΔR_c, is then simply

$$\Delta R_c = R_{int} - R_c \, , \tag{4.2}$$

where R_c is the reflectance at the band center. The central and shoulder wavelengths for the four absorption bands are listed in Table 4.1 and illustrated in Figure 4.1. The selection of shoulder wavelengths was based on the shape of the dry sample curves for the 1440 nm and 1930 nm bands, while the shoulder wavelengths for the 970 nm and 1160 nm bands and the central wavelengths for all bands were determined from minima of the saturated sample curves.

Table 4.1: Absorption band centers and shoulders

No.	I	II	III	IV
Band center	970 nm	1160 nm	1440 nm	1930 nm
Left shoulder	930 nm	1120 nm	1380 nm	1850 nm
Right shoulder	1080 nm	1270 nm	1680 nm	2130 nm

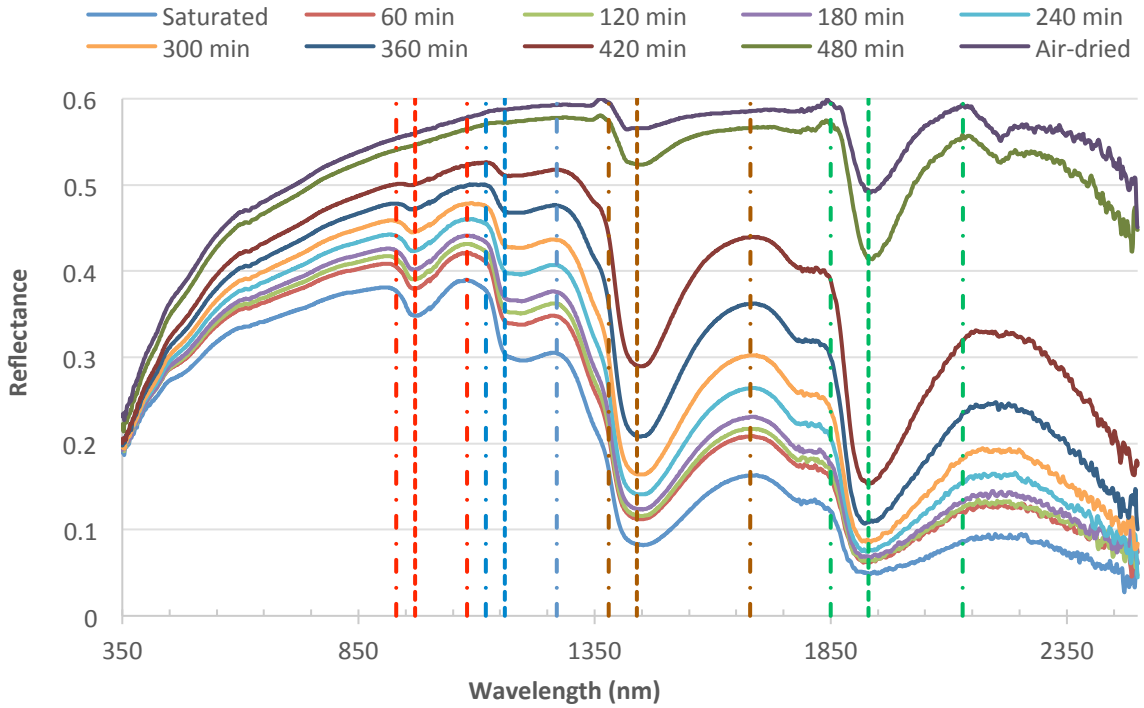

Figure 4.1[1]: The spectral reflectance of white sand changes with changing moisture content. Dashed lines mark the centers of the absorption bands; dashed dotted lines mark the band shoulders. Solid line shows linear interpolation between shoulders for the 1930 nm absorption feature.

[1] The shape is different from Figure 4.3 of the same sample. The FOV here exceeds sample area. It doesn't influence this study on band depth, a relative value.

4.2 Volumetric water content

Soil moisture content is normally described by either gravimetric or volumetric water content. Due to the different water storage capacity of the three soil samples, gravimetric water content will vary over a large range. In contrast, volume water content is normalized by the volume of sample holder, which is in a narrower range and is also more comparable to other studies (Lobell & Asner 2002; Liu et al. 2002).

The equation for calculating volumetric water content is:

$$\theta = \frac{V_{water}}{V_{total}} = \frac{m_{water}}{\rho_{water} \cdot V_{total}}, \tag{4.3}$$

where θ is the volume water content (VWC), V_{water} is the water volume, V_{total} is the total volume of solids, water, and air space, m_{water} is the water mass, and ρ_{water} is the water density (1.0 g/cm^3).

4.3 Sample depth

Given the small depth of the sample, it was important to determine that the sample was optically deep, i.e., deep enough that no light was reaching the bottom and that reflectance from the bottom would not affect the reflectance measurements. Reflectance from dry soil is very much a surface phenomenon in that the reflected light derives from the first several millimeters of the soil surface (Liang 1997). Because wetting the soil increases forward scattering (Neema et al. 1987), this will increase the depth of light penetration. In order to test light penetration through white sand – the most transmissive of the soil samples – and water, and certify that the depth of the soil sample is sufficient to prevent reflectance from the bottom of the sample holder influencing observed reflectance, colored tapes (red and orange) were used to add a strong

spectral feature to the bottom reflectance. Visible wavelengths are appropriate because water is most transmissive in the visible (Kou et al. 1993). The soil reflectance was also lowest in the visible, allowing for the best contrast in reflectance. With red tape covering the inside bottom of the sample holder, the spectral reflectance of the exposed tape showed a steep increase from less than 0.1 at 550 nm to over 0.55 at 650 nm for the red tape with the steepest slope at ~600 nm. With the orange tape, the reflectance increased from less than 0.1 at 450 nm to more than 0.65 at 600 nm with the steepest slope at ~575 nm (Figure 4.2). The spectral increase is abrupt and is an easily identifiable "color feature" that should be apparent if bottom reflectance is contributing to the overall reflectance signal.

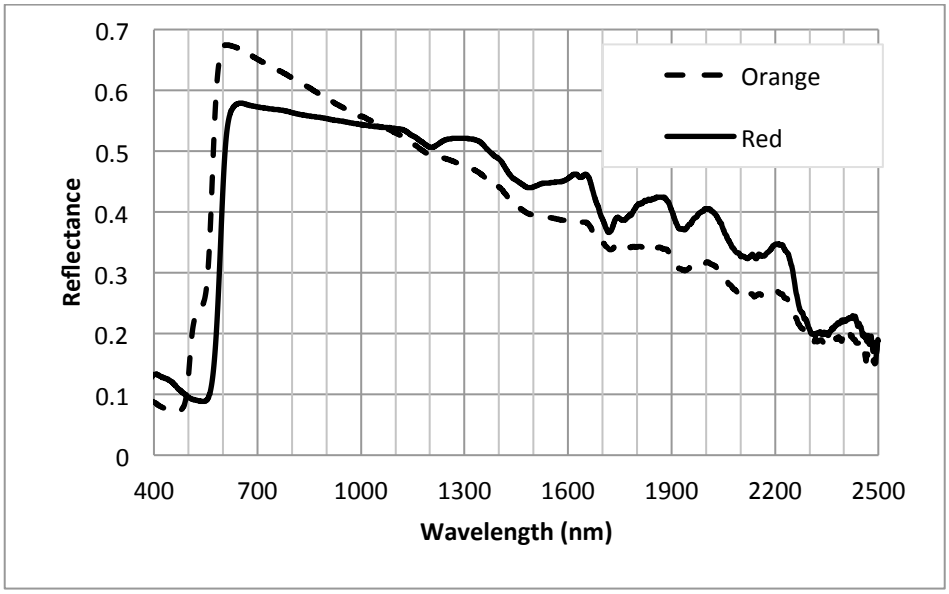

Figure 4.2: Spectral reflectance of bottoms of sample holder covered by red and orange tape, respectively.

To ensure that 1.2 cm, the depth of sample holder is enough, a further verification was executed. In the verification, reflectance of two dry quartz sand samples with 1 cm-deep and 2 cm-deep were collected, as shown in Figure 4.3. These two reflectance curves are equivalent, and no color feature shows, which means 1 cm-deep quartz sand is enough to reflect and absorb

all light. Furthermore, collected spectral reflectance data only present soil/water feature without sample holder bottom information. The measured reflectance only shows reflectance features of soil during the drying process; as a result, a 1 cm-deep quartz sand sample is used in this study.

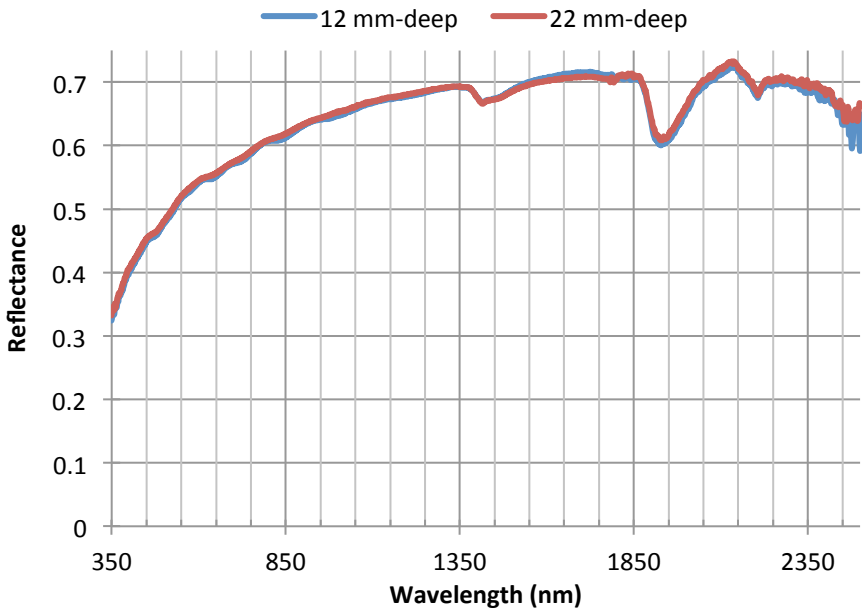

Figure 4.3: Reflectance of 1 cm and 2 cm thick dry quartz sand .

5. Results

Figure 5.1 shows spectra of the three soil samples collected at hourly intervals during the drying process. Reflectance is highest at all wavelengths and for all soils when the samples are dry, with reflectance in the infrared consistently higher than in the visible. With increasing water content, reflectance decreases at all wavelengths, but the response is more dramatic in the infrared. Moreover, the decreases in reflectance at the center of the major water absorption bands, centered at 1440 nm and 1930 nm, are particularly strong for all three soils. This is in striking contrast to the minor water absorption bands centered at 970 nm and 1160 nm, which can only be observed in the quartz sand spectra.

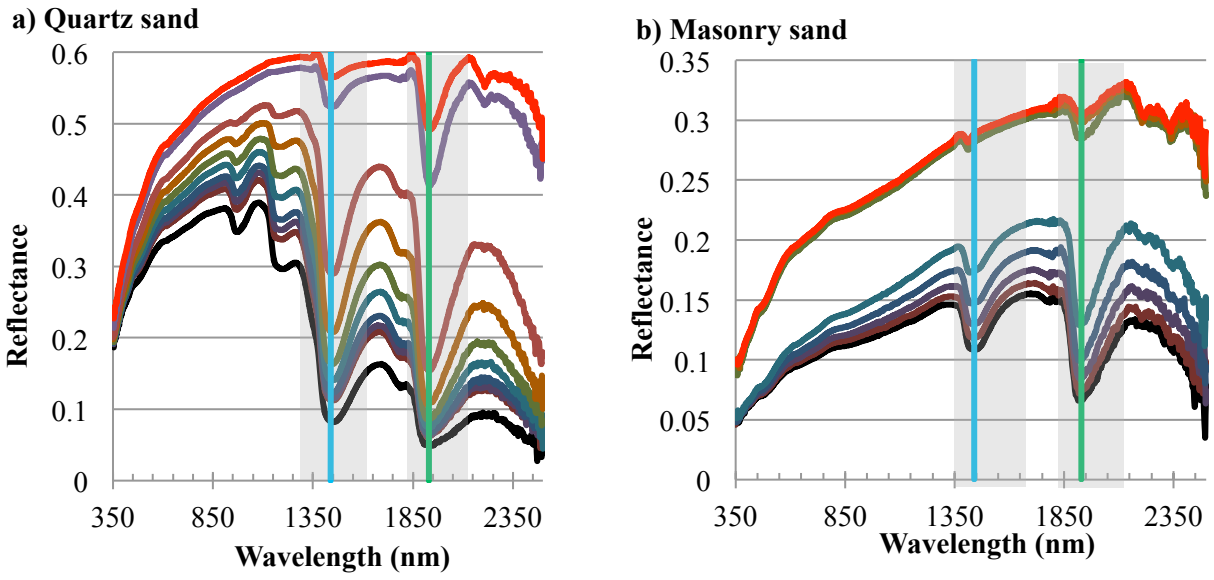

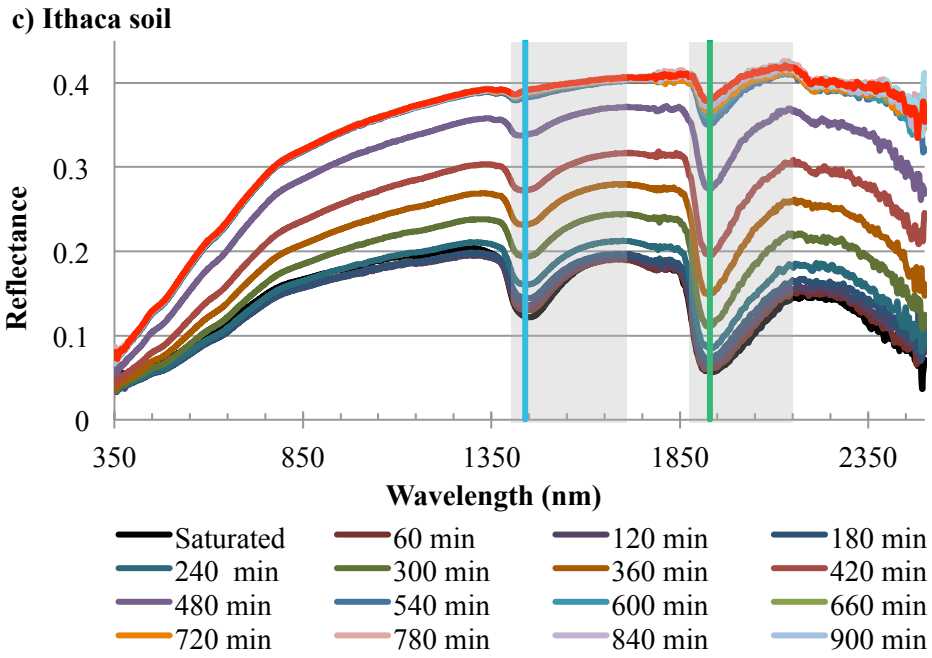

Figure 5.1: Spectral reflectance changes with changing water content from saturated to air-dry. The time interval between spectra is 60 minutes. Solid lines mark the centers of the major absorption bands; grey strips mark the band shoulders. a) quartz sand dried for 510 minutes, b) masonry sand dried for 480 minutes, and c) Ithaca soil dried for 1020 minutes, shrinking significantly during the late segment drying.

Some general features in the reflectance spectra are consistent for all three soils during the drying process: 1) reflectance in the infrared is more sensitive to water content changes; 2) the change in reflectance at the SWIR water absorption bands is more dramatic; 3) the 1930 nm absorption band is always deeper than other absorption bands; 4) reflectance change is slower during the first few hours of the drying period, then becomes more rapid.

Other features in the reflectance spectra are not as consistent among the three soils. For instance, the water absorption bands at 970 nm and 1160 nm appear in the wet quartz sand reflectance, but are missing in the wet reflectance spectra for other two soils. The sequence of changes in reflectance also differs greatly among the three soils. For quartz sand, reflectance increases in the first 60 minutes of drying, stabilizes for two hours, and then increases steadily

for the next four hours until near the end of the drying period when reflectance increases sharply. For the masonry sand, the reflectance increase begins slowly, accelerates steadily but slowly over the first four hours, and then increases dramatically to nearly air-dried reflectance except for water absorption bands in the infrared. It then takes another three hours to reach the air-dried condition. The reflectance of Ithaca soil remains quite dark for the first four hours after saturation. The reflectance then increases relatively steadily for five hours reaching a nearly air-dried condition. For the last nine hours, the most apparent change in reflectance spectra is the 1930 nm water absorption band. The strong change in absorption bands suggest they will be an effective indicator for characterizing soil water content, even toward the end of the drying process.

The change in band depth over the full drying period for the two absorption bands in the SWIR region is shown in Figure 5.2. For all three soil samples, there is an abrupt decrease in the band depth for these two bands as the samples dry. Except for this obvious decrease, during the whole process, the band depth changes smoothly. The band depth centered at 1930 nm is normally deeper than the 1440 nm band depth, and the 1930 nm band depth is changing over a wider magnitude than at 1440 nm, which means the 1930 nm band is more sensitive to changing water content.

However, as is seen in Figure 5.2, neither the magnitude, nor the change in magnitude of the same absorption band is similar among three soils. The abrupt decrease occurs at different times (probably a different water content, too), which suggests that any relationship between water content and absorption band depth will not be independent of soil characteristics.

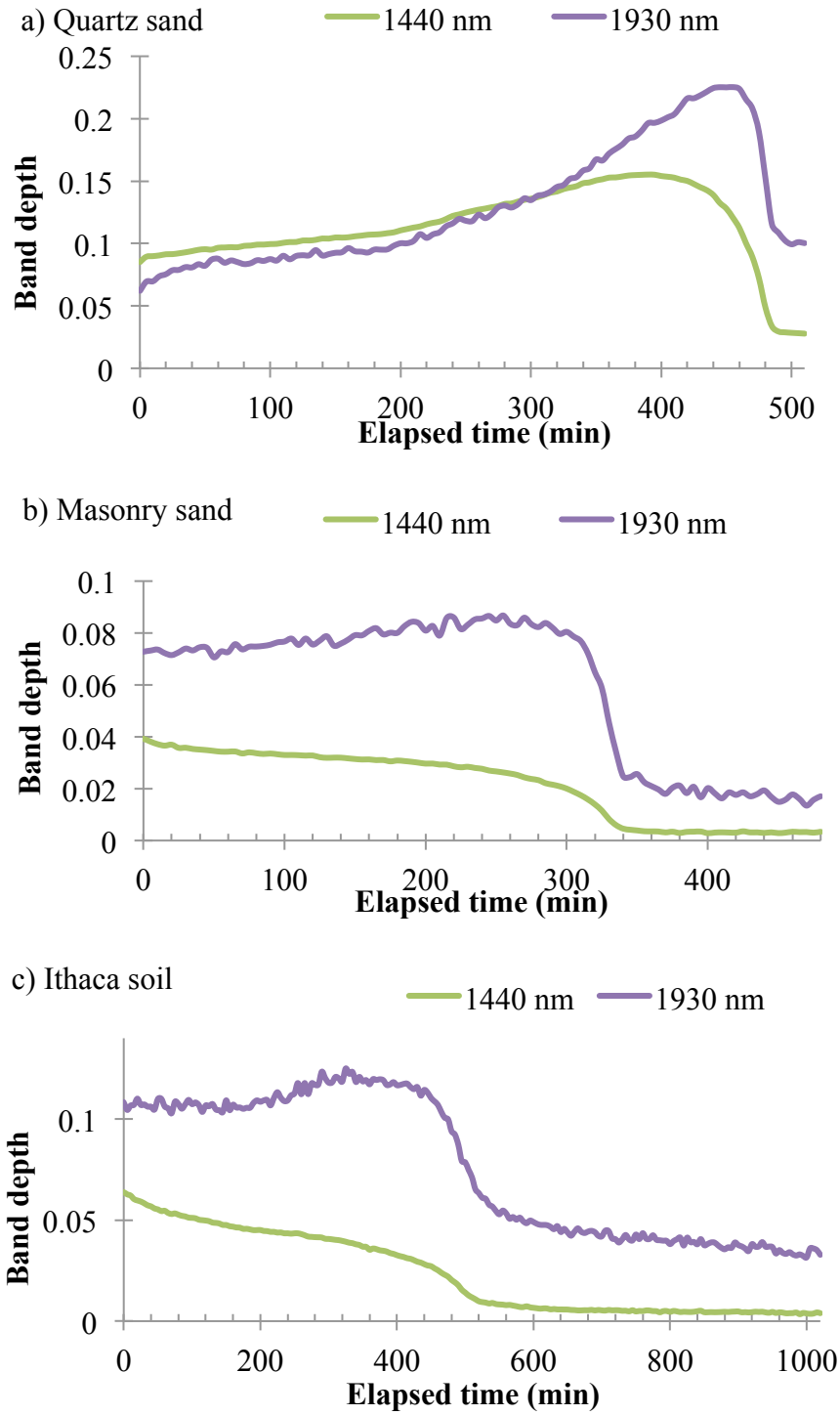

Figure 5.2: Changing band depth centered at 1440 nm and 1930 nm versus elapsed time. Among three soil sample, the features are different.

5.1 Band depth segmentation

To analyze the band depth thoroughly, the absorption band depth for each soil sample is segmented into several parts. From Figure 5.2, the band depth change is obviously different among different soils. The goal is to characterize the similarities and differences in order to develop a hypothesis or explain the features.

In order to compare the changing band depths, ΔR_c (Equation (4.2)), plots of the two absorption bands in the SWIR are segmented and fit to straight lines for all three soil samples. The linear fitting results for the different soil samples are shown in following separate sections. For all water absorption band depth curves from the three samples, there is a small, nonlinear transition period which is treated separately. During the last drying segment for all three samples, the water absorption band depth changes only slightly with decreasing water content, and is strongly influenced by noise.

5.1.1 Quartz sand

Table 5.1 and Table 5.2 show the fitting results for the 1930 nm and 1440 nm band depth respectively. The fitting excludes the short, highly non-linear period prior to the abrupt decrease. Except for the end of drying process, the segmented linear fittings are highly correlated, with R^2 all above 0.9. For the last segmentation, band depth changes over a small range, which may exceed the measurement accuracy.

Table 5.1 Band depth at 1930 nm segments fitted with linear relationship for quartz sand

Segment	Time	Linear fitting	R^2
A	0-240 min	$y = 1.47 * 10^{-4}x + 0.073$	0.92
B	240-450 min	$y = 5.82 * 10^{-4}x - 0.035$	0.99
C	460-490 min	$y = -4.56 * 10^{-3}x + 2.343$	0.98
D	490-510 min	$y = -1.87 * 10^{-4}x + 0.196$	0.68

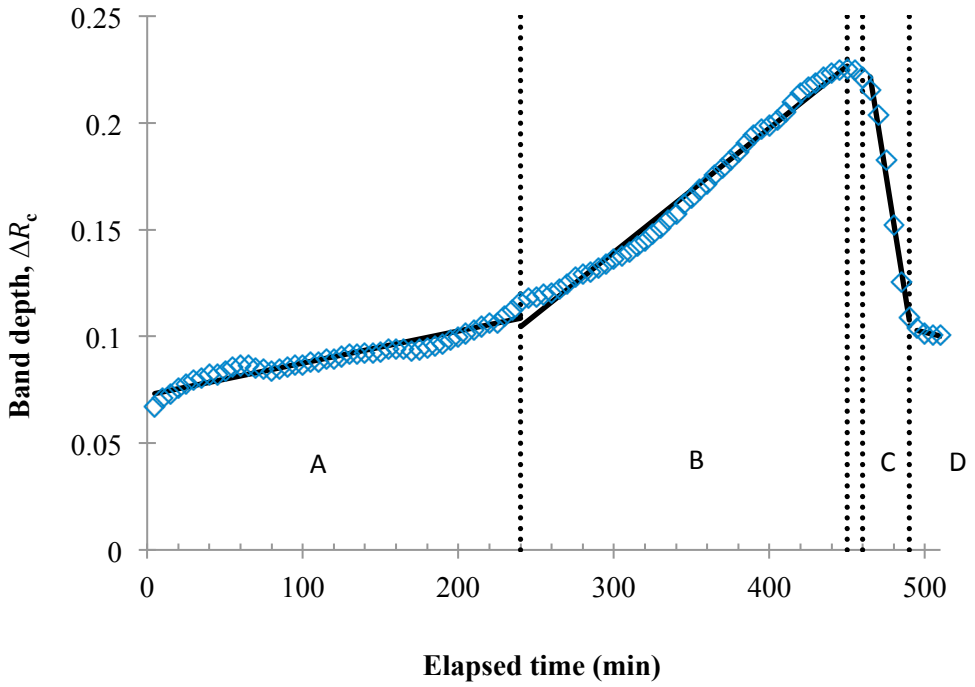

Figure 5.3: Changing band depth centered at 1930 nm of quartz sand during drying process (blue open diamonds), and segmented linear fitting solid lines as shown in Table 5.1. Dotted lines mark break points for each segment, and the segments are labeled.

Table 5.2 Band depth, ΔR_C, at 1440 nm segments fitted with linear relationship for quartz sand

Segment	Time	Linear fitting	R^2
A	0-190 min	$y = 9.96 * 10^{-5}x + 0.089$	0.90
B	190-390 min	$y = 2.52 * 10^{-4}x + 0.061$	0.99
C	440-480 min	$y = -2.30 * 10^{-3}x + 1.164$	0.96
D	480-510 min	$y = -3.11 * 10^{-4}x + 0.185$	0.66

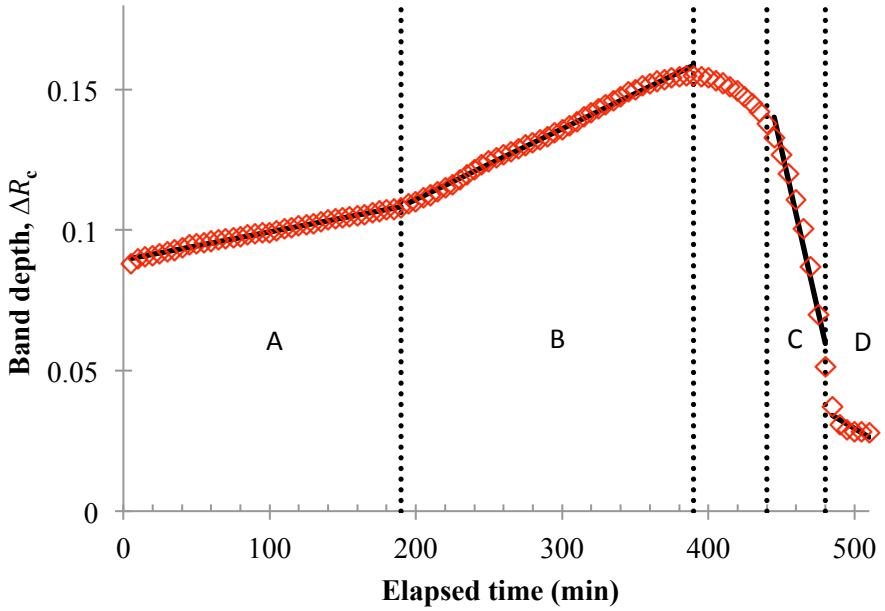

Figure 5.4: Changing band depth centered at 1440 nm of quartz sand during drying process (red open diamonds), and segmented linear fitting solid lines as shown in Table 5.2. Dotted lines mark break points for each segment, and the segments are labeled.

For quartz sand, both absorption band depth curves are separated into four segments for linear fitting. The excluded transition period between the second and third segments begins earlier and lasts longer at 1440 nm than at 1930 nm. Also, the band depth at 1930 nm is initially shallower, but becomes deeper than at 1440 nm when approaching the end of drying, and

remains higher when soil is air-dry. Note that the final segment (D) in the band depth change for quartz sand is very short at both 1440 nm and 1930 nm.

5.1.2 Masonry Sand

Table 5.3 and Table 5.4 show the fitting result for 1930 nm and 1440 nm respectively, with corresponding graphs in Figure 5.5 and Figure 5.6. As shown in the quartz sand fitting, the last segment is the least correlated part, especially at 1440 nm. For masonry sand, the break points for the two absorption bands don't differ greatly. The extreme low R^2 for the 1440 nm band may be caused by the relatively smaller band depth change, which barely exceeds the measurement accuracy over the whole segment.

For the Masonry sand, both absorption bands are separated into three segments for linear fitting. For this soil, the absorption band at 1930 nm is consistently deeper than 1440 nm throughout the drying period, and remains higher when soil is air-dry. For masonry sand, there is no change in slope during the early drying period as there was with quartz sand, thus, segment-A is abandoned. The depth change during in segment-B is long and steady, and segment-C is very strong and rapid. The most obvious difference from the quartz sand is in segment-D, which lasts more than 200 minutes for both absorption bands, with band depth changing only slightly.

Table 5.3: Band depth at 1930 nm segments fitted with linear relationship for masonry sand

Segment	Time	Linear fitting	R^2
B	0-250 min	$y = 5.58 * 10^{-5}x + 0.071$	0.88
C	300-340 min	$y = -1.58 * 10^{-3}x + 0.568$	0.96
D	340-480 min	$y = -5.53 * 10^{-5}x + 0.041$	0.69

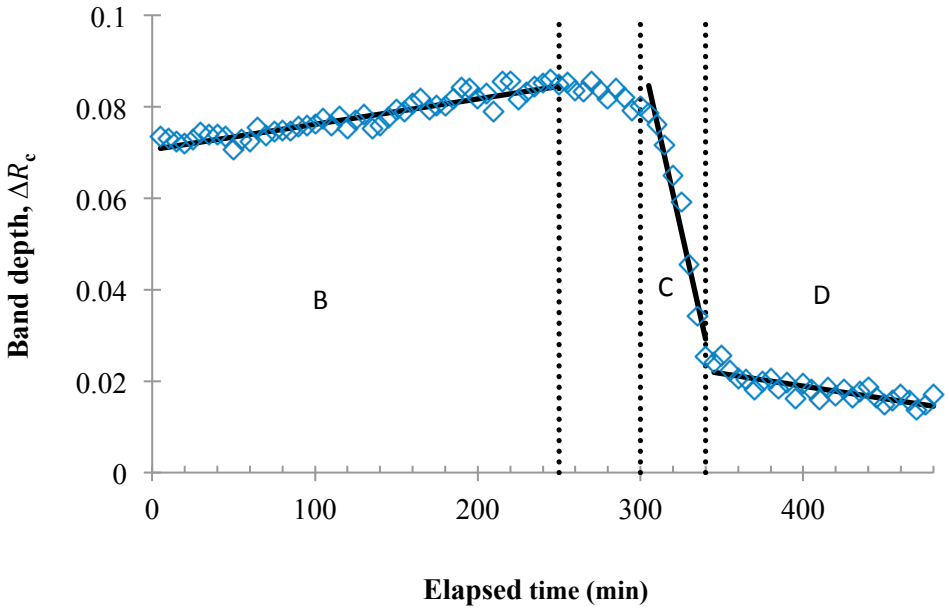

Figure 5.5: Changing band depth centered at 1930 nm of masonry sand during drying process (blue open diamonds), and segmented linear fitting solid lines as shown in Table 5.3. Dotted lines mark break points for each segment, and the segments are labeled.

Table 5.4: Band depth at 1440 nm segments fitted with linear relationship for masonry sand

Segment	Time	Linear fitting	R^2
B	0-250 min	$y = -3.72 * 10^{-5}x + 0.037$	0.98
C	300-330 min	$y = -4.09 * 10^{-4}x + 0.144$	0.98
D	330-480 min	$y = -7.97 * 10^{-6}x + 0.007$	0.37

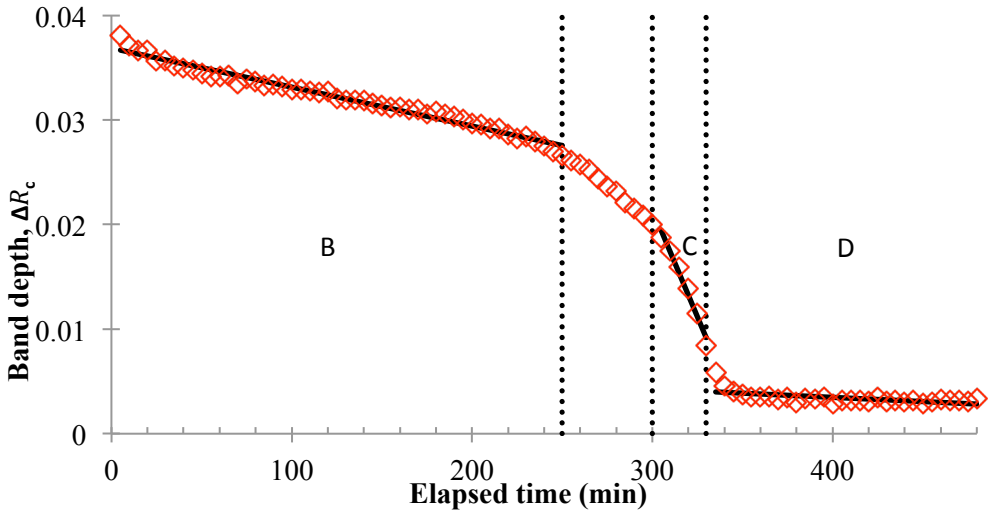

Figure 5.6: Changing band depth centered at 1440 nm of quartz sand during drying process (red open diamonds), and segmented linear fitting solid lines as shown in Table 5.2.2. Dotted lines mark break points for each segment, and the segments are labeled.

5.1.3 Ithaca soil

Figure 5.7 and Figure 5.8 show the fitting result for 1930 nm and 1440 nm respectively, and the fitting results are shown in Table 5.5 and Table 5.6. The fitting results differ for the two absorption bands. For the 1930 nm band, the least correlated segment is segment-B, while the other two segments both have $R^2 > 0.90$, however. For 1440 nm, the least correlated segment is segment-D with R^2 equaling 0.81.

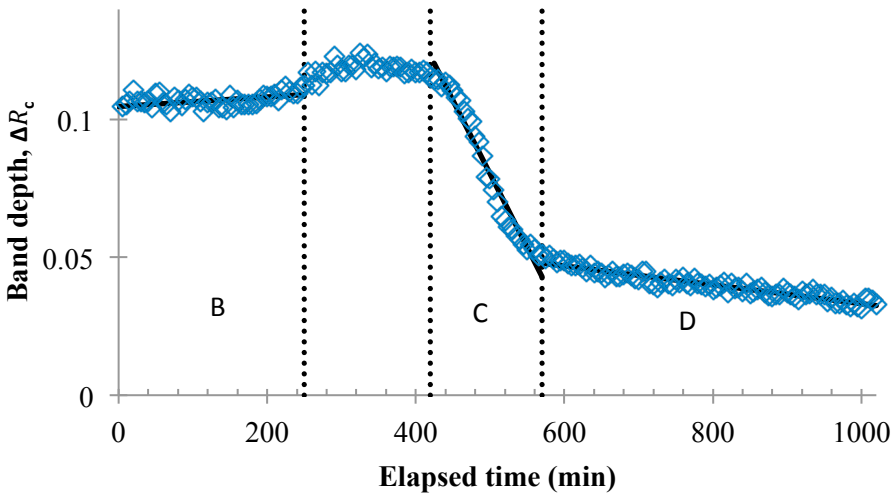

Figure 5.7: Changing band depth centered at 1930 nm of Ithaca soil during the drying process (blue open diamonds), and segmented linear fitting solid lines as shown in Table 5.5. Dotted lines mark break points for each segment, and the segments are labeled.

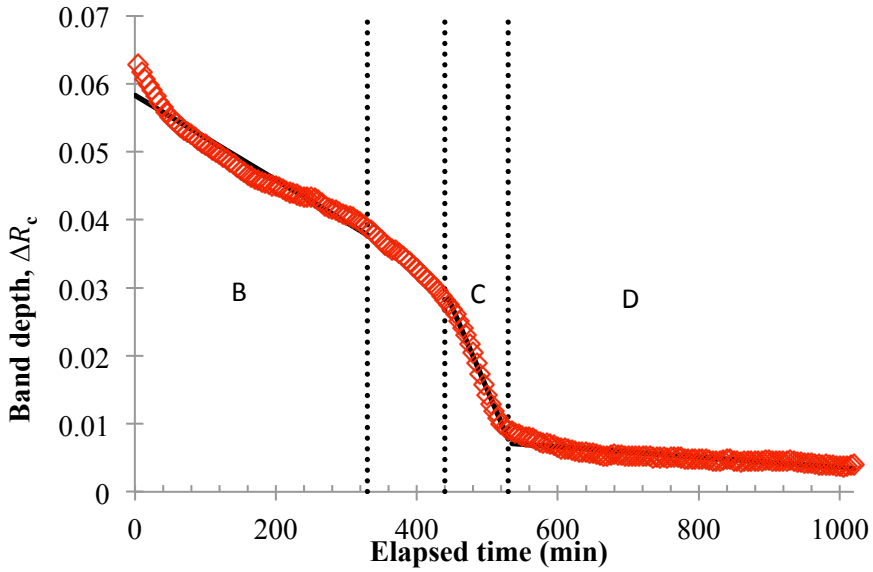

Figure 5.8: changing band depth centered at 1440 nm of Ithaca soil during the drying process (red open diamonds), and segmented linear fitting solid lines as shown in Table 5.6. Dotted lines mark break points for each segment, and the segments are labeled.

Table 5.5: Band depth at 1930 nm segments fitted with linear relationship for Ithaca soil

Segment	Time	Linear fitting	R^2
B	0-250 min	$y = 1.76 * 10^{-5}x + 0.105$	0.24
C	420-570 min	$y = -5.34 * 10^{-4}x + 0.347$	0.97
D	570-1020 min	$y = -3.41 * 10^{-5}x + 0.067$	0.91

Table 5.6: Band depth at 1440 nm segments fitted with linear relationship for Ithaca soil

Segment	Time	Linear equation	R^2
B	0-330 min	$y = -6.23 * 10^{-5}x + 0.058$	0.95
C	440-530 min	$y = -2.42 * 10^{-4}x + 0.136$	0.99
D	530-1020 min	$y = -7.54 * 10^{-6}x + 0.011$	0.81

As delineated in Figure 5.7 and Figure 5.8, both absorption bands are segmented into three parts for linear fitting. For Ithaca soil, the band depth at 1930 nm during segment-B is nearly constant, explaining the poor correlation. At 1440 nm the change in band depth is nearly linear except for the very beginning. For both bands, the excluded transition period is much longer than for the other two soil samples. Segment-C lasts only a short time, which is consistent among all three soils, but a much longer time is required for evaporation during segment-D. Segment-D lasts near 500 minutes, the longest time among all soil samples. During this time, the band depth for both absorption bands changes only slightly.

Comparing all three soil samples from the above tables and figures, one striking differences is that the quartz sand band depths (at both 1930 nm and 1440 nm) have two distinct segments spanning the initial drying process although, curiously, the timing of the segments do not coincide. In contrast, the rates of change for the masonry sand and Ithaca soil fluctuate, but

do not appear to have clearly defined segments within the initial period. For the 1440 nm band, the most apparent difference between quartz sand and the other two samples is that the band depth is increasing as the water evaporates, but for other two samples, the band depth decreases monotonically during the whole sequence. Another important difference among the samples is the length of segment-D. For quartz sand, segment-D is short, while for Ithaca soil, the segment-D occupies nearly half of the total drying time, and masonry sand is intermediate.

One similarity shared among three varied samples is that the changing band depth at 1440 nm is always smoother (less noisy) than the band depth at 1930 nm. So the 1440 nm should be more appropriate to build a relationship between soil water content and spectral absorption features.

The absorption band depth is most sensitive to water content change during segment-C for all three samples. In contrast, the patterns of change are quite different at the beginning and the end of drying. The differences at the beginning are likely to be a result of unstable evaporation. On the other hand, at the end, the measurement accuracy is not enough to collect data beyond noise, resulting in unstable measurements.

All in all, the break points in the band depth curves occurred at different times among three varied types of soil, and also differed for the two wavelengths. The reflectance magnitude also differed due to soil physical features. Though it's hard to summarize specific drying features common to all three soil types, the changing band depths of three samples actually share similar tendencies. The continuous band depth change can be segmented into similar, roughly linear segments. During the last segment, the water content changes slowly for all three soils, but the drying times differ markedly. In order to gain a better understanding of the similarities of the

band depth changes, the relationship between reflectance feature (band depth) and water content is studied further.

5.2 Band depth and VWC

In section 5.1, band depth is analyzed in the time domain, which is reasonable intuitively and direct. However, because the water-holding capacity varies among different types of soil, and the duration time for drying is different, the time domain is not the most appropriate metric to compare drying features among different types of soil. Our purpose for this study is to examine the relationship between the water absorption band depths and water content, so VWC is introduced as a preferred metric of water content.

Table 5.7 lists the VWC for saturated soils along with the total elapsed time of drying from saturation to air-dry. In Table 5.7, high VWC results in longer drying time. However, for the Ithaca soil, the duration of drying lasts about twice as long as the other samples despite a relatively small increment in maximum VWC. The longer time required for the drying process may be caused by the high-ratio clay content in the Ithaca soil, with the binding between clay and water tending to keep water from escaping into air.

Table 5.7: Maximum VWC and total drying time for three soils

	Max. VWC	Elapsed time for drying
Quartz sand	0.390	510 min
Masonry sand	0.351	480 min
Ithaca soil	0.536	1020 min

In section 5.1, the changes in band depths centered at 1440 nm and 1930 nm were separated into segments. Table 5.8 summarizes the VWC and band depth changes during the different segments. For Quartz sand, the band depths at both 1440 nm and 1930 nm increase as water evaporates. For both bands, more than 80% of the water evaporates in segment-A and segment-B while the band depth increases. In segment-C and segment-D, less than 10% of the initial water escaped, yet the depth decrease was equivalent to the increase during segments-A and segment-B. For masonry sand, nearly 70% of the total water evaporates with relative slight band depth change in Segment-B. Less than 20% water evaporates in segment-C and segment-D, but the depth changes for both bands are more pronounced than in segment-B. Similar to masonry sand, Ithaca soil band depths at 1440 nm and 1930 nm change slowly in segment-B though more water evaporates compared to segment-C and segment-D. For the 1930 nm band, the band depth changes only slightly until about 40% water has evaporated during segment-B. In segment-C and segment-D, the total loss of water is equivalent to the quantity lost in segment-B, but the depth change is more pronounced. Moreover, water loss in each segment between segment-C and segment-D is about 17%, while the changed depth is still more apparent in segment-C. At 1440 nm band, segment-C also exhibits the most pronounced rate of change of the band depth.

To summarize the above observations, contrary to expectation, the changing amount of water does not consistently influence the water absorption band depth. For example, in segment-C, though just a small amount of water evaporated, the band depth decreased strongly. This indicates that the water amount is not controlling the band depth changes.

Table 5.8: Changes in band depths centered at 1440 nm and 1930 nm with decreasing VWC for each soil sample.

	Quartz sand				Masonry sand				Ithaca soil			
	1930 nm		1440 nm		1930 nm		1440 nm		1930 nm		1440 nm	
Segment	VWC %	Band depth	VWC %	Band depth	VWC %	Band depth	VWC %	Band depth	VWC %	Band depth	VWC %	Band depth
A	51.8%	0.049	41.0%	0.020	-	-	-	-	-	-	-	-
B	42.3%	0.109	41.8%	0.047	68.7%	0.013	68.7%	-0.013	39.6%	0.008	51.9%	-0.024
C	3.3%	-0.112	6.4%	-0.087	9.4%	-0.055	7.7%	-0.012	17.2%	-0.065	10.8%	-0.019
D	0.8%	-0.008	1.3%	-0.023	8.8%	-0.008	10.5%	-0.005	17.9%	-0.017	21.5%	-0.005

The changes in band depth over the full drying period for all four absorption bands is shown in Figure 5.9 for each of the three soils, along with the change in VWC. For all three soils, the change in VWC is nearly linear until the very end of the drying period, indicating a constant evaporation rate typical of soils drying under constant temperature and humidity. For the quartz sand, the band depths for the weaker absorption bands (970 nm and 1160 nm) decrease monotonically with time, coincident with the decrease in VWC. The change in band depth is slight for the first 200 minutes, but changes somewhat more rapidly as the sample dries. For the masonry sand and Ithaca soil, the 970 nm and 1160 nm bands are not readily apparent in the reflectance spectra and changes in band depths are negligible.

Because water absorption bands at 970 nm and 1160 nm are not commonly observed in all three soil sample, absorption bands at 1440 nm and 1930 nm are selected as the most promising features. In Figure 5.9, the 1930 nm absorption band is the most pronounced feature for all three soils. An important, common characteristic is that the depth of the 1930 nm

absorption band initially increases steadily, reaches a maximum, and then decreasing abruptly. At 1440 nm, the band depth also initially increases for the quartz sand, more gently than that at 1930 nm. In contrast, the 1440 nm band depth decreases monotonically for the masonry and Ithaca soil. The common point is a relatively abrupt decrease appearing in all three soils.

Although the time required for drying differs substantially and the details of the changes in band depth are quite different for the three soils, the rate of change in VWC is constant for the bulk of the drying period in all cases. For all three soils, the transition from a constant rate of change in VWC to a much slower rate at the end of the drying period coincides consistently with the dramatic changes in the band depth at 1930 nm.

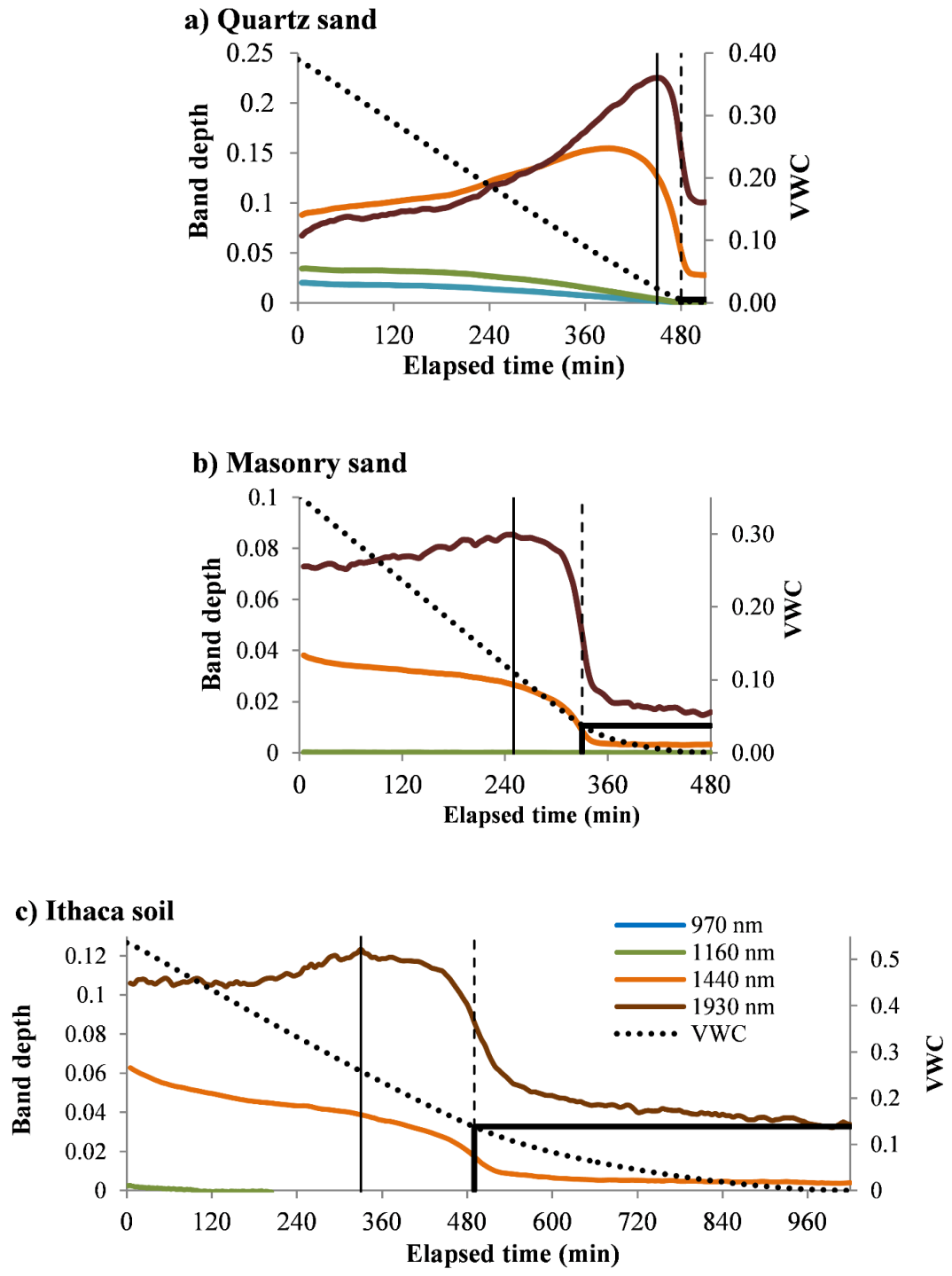

Figure 5.9: Change in band depth (colored lines) and VWC (dotted black line) with elapsed time from saturation to air-dry; a) quartz sand, b) masonry sand, c) Ithaca soil. The solid vertical line indicates the maximum band depth at the 1930 nm; the dashed vertical lines indicate the minimum (negative) slope at 1930 nm. The heavy black solid lines mark the time and VWC values that coincide with the minimum slope.

Table 5.9 shows the elapsed time and corresponding VWC at maximum band depth for three soils. Relating this pattern to the drying segment discussion of drying process (Sections 5.1, 5.1.2, and 5.1.3), the maximum band depth occurs at the end of segment-B for quartz sand and masonry sand, and during the unclassified transition between segment-B and segment-C for Ithaca soil.

Table 5.9: Elapsed time and VWC at maximum band depth for three soils

	Minimum slope time	VWC
Quartz sand	480 min	0.006
Masonry sand	330 min	0.039
Ithaca Soil	490 min	0.144

As expected, the absorption band depth was quite sensitive to the VWC, especially in unsaturated conditions. In Figure 5.10, the most sensitive and apparent band depth, centered at 1930 nm, is plotted versus VWC. Contrary to expectations, however, the change in band depth with moisture content was far from consistent among the three soil types. Indeed, the magnitude of the maximum band depth varies by almost a factor of three. Even more surprisingly, the band depth did not decrease monotonically with decreasing moisture; rather, band depth increased with decreasing moisture content for higher VWC, and then decreased rapidly during the later segment of drying (Figure 5.10). The pattern is markedly different for each of the soils. In particular, the maximum band depth occurs at widely different values of VWC. The one consistent characteristic is that the band depth increases relatively slowly during most of the drying period, and decreases more rapidly over a relatively short range of VWC. This also indicates that the amount of water is not the main factor influencing absorption band depth, but

rather is controlled by the water distribution in the soil or the water loss pattern during the drying process.

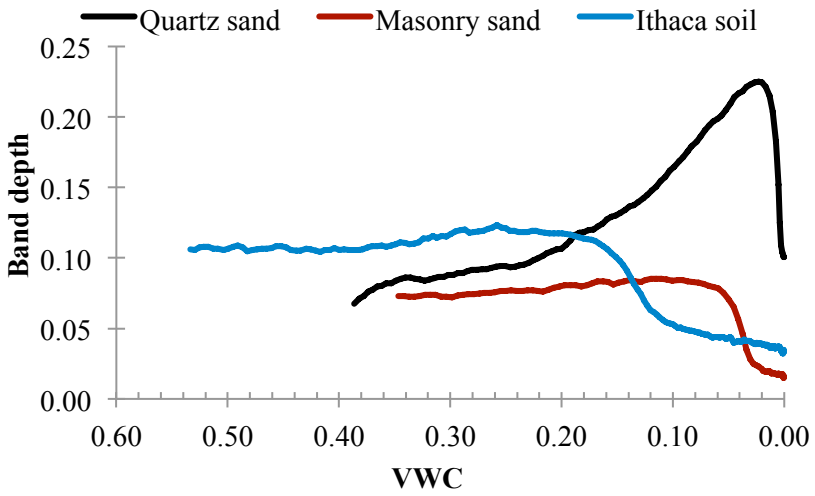

Figure 5.10: Variation of the band depth at 1930 nm with VWC for the three soil types.

While the magnitude of the band depth – especially the maximum band depth – may be related to differences in the magnitude of the reflectance among the three soil types, the differences in the shapes of the curves and the location of the maximum are more likely to be related to the soil structure (pore sizes, particle size distribution) and the distribution of the water at the soil surface.

5.3 Rate of change in band depth and evaporation

The results of the experiment indicate that the initial hypothesis that absorption band depth is only related to water content and independent of soil type is not correct. However, in Figure 5.9, the 1440 nm and 1930 nm band depth of each soil change at close to the same time, and the band depth change and decrease in the VWC slope (slowing of evaporation) also occur around the same time. This indicates changing evaporation rate can be a factor relating to absorption band depth beyond soil types. The rate of evaporation controls the rate of water loss,

and is compared to the rate of changing band depth, calculated in this section, in order to examine the relationship between soil water content and drying features in spectral reflectance.

The changing depth of the water absorption bands may be useful as an indicator of the change in evaporation rate. In order to examine this idea, the evaporation rate is calculated for each soil. To present evaporation rate intuitively, elapsed time during drying is used as the metric in this section. As shown in Figure 5.11 a) and b), the rates of changing band depth of two of the absorption bands (1440 nm and 1930 nm) are nearly zero for the first 400 and 300 minutes, respectively, and reach a minimum at nearly the same time for both bands. In Figure 5.11 c), the rate of change in band depth is also near zero for the first 400 minutes for both bands, although the 1930 nm signal is very noisy. Once more, the minimum occurs at nearly the same time for both bands, but in the middle of the whole drying process. Table 5.10 lists the time of occurrence of the maximum rate of change in band depth for both the 1440 nm and 1930 nm bands. The maximum difference for the two bands is only 10 minutes, so the following discussion will focus on the 1930 nm band.

Table 5.10: Elapsed time at maximum rate of changing band depth for different soils

Band	Quartz sand	Masonry sand	Ithaca soil
1440 nm	480 min	330 min	500 min
1930 nm	480 min	335 min	490 min

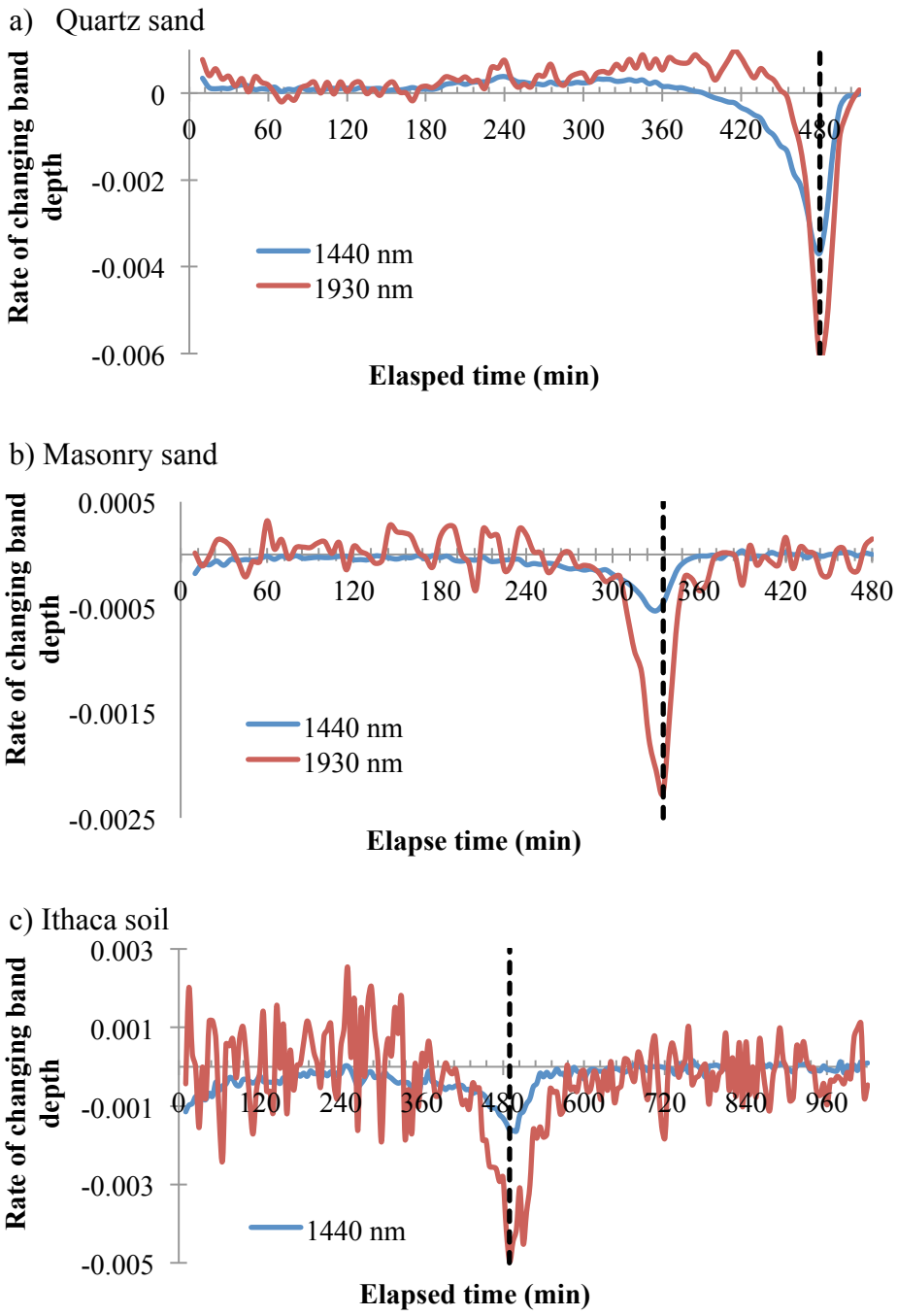

Figure 5.11: The rate of changing water absorption band depth at 1440 nm and 1930 nm, with the dashed lines marking the maximum rate of change in the 1930 nm band depth.

Figure 5.12 presents the evaporation rate, calculated as a 15-minute running average. The initial evaporation rate was nearly constant, and ranged between 0.0010 and 0.0012

$g \cdot cm^{-2} \cdot min^{-1}$ for all three soils. This initial, steady-state period corresponds to segment-B (and segment-A for the quartz sand) drying (Lehmann et al., 2008), a period during which the soil particles are hydraulically connected with a nearly constant water content at the surface, and continuously replenished through a network of water films connecting the pore spaces.

The consistency of the behavior of the 1930 nm band depth and its correspondence to the transition between stage-1 and stage-2 drying is rather surprising given the differences among the three soil samples. The average particle sizes were very different. The quartz sand consisted predominantly of particles that were 0.05 mm or more in size. The Ithaca soil (silty loam) contained very little sand and much more clay (particle size < 0.002 mm), and shrank significantly during stage-2 drying, leaving a roughly 1 mm space around the edge of the sample holder. The average particle size of the Masonry sand (coarse sand) was intermediate between the other two. In addition, the actual amount of water present in the samples at the time of the transition varied by over an order of magnitude (Table 5.9). This implies that, regardless of the particle size (or pore size) distribution, the disposition of water at the soil surface is somehow similar for all soils during the transition between stage-1 and stage-2 drying.

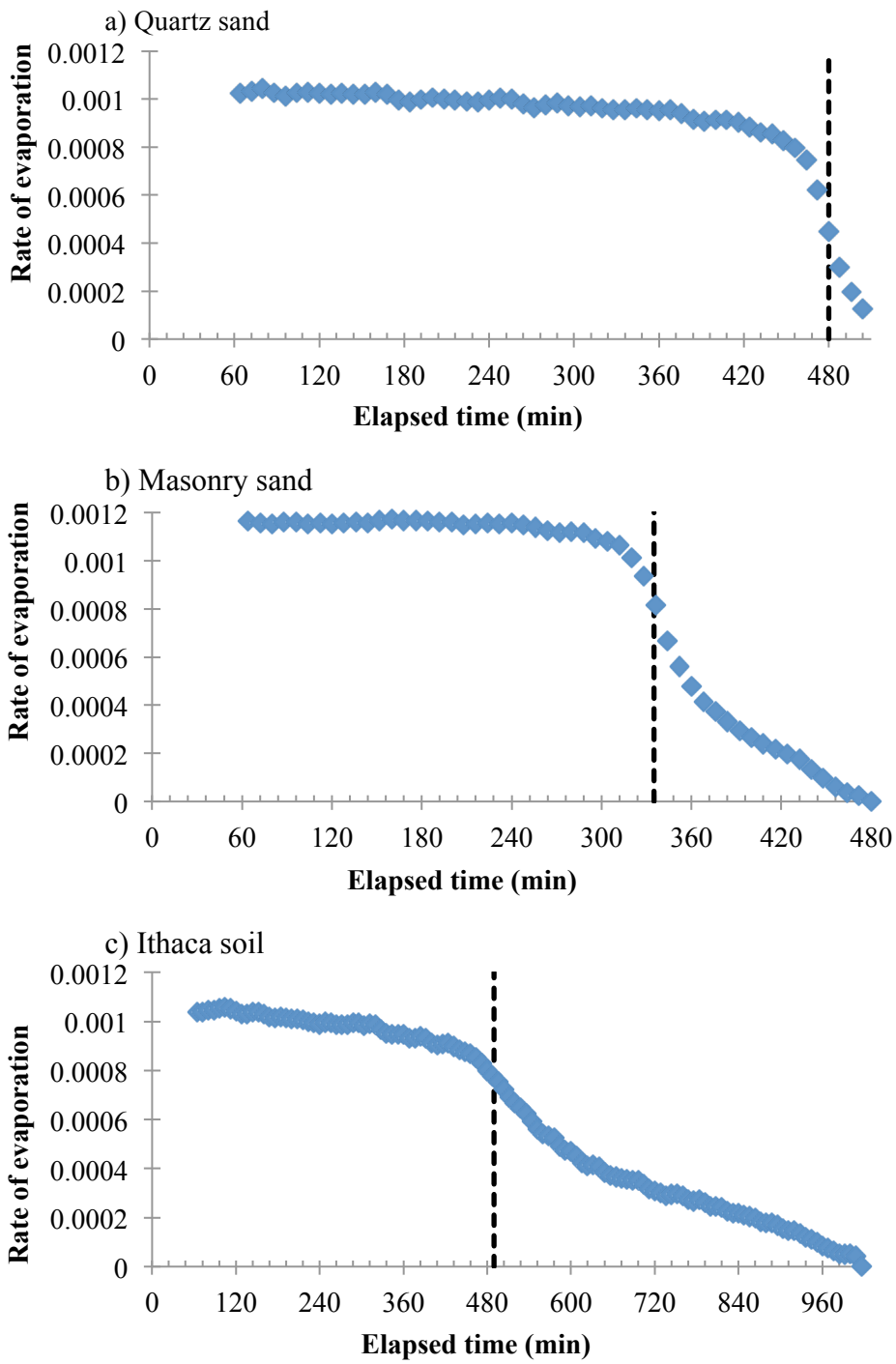

Figure 5.12: Evaporation rate throughout the drying period for the three soils. The solid vertical line represent the maximum band depth for the 1930 nm absorption band; the dashed line marks the time of most rapid change in the band depth for the 1930 nm absorption band. Elapsed time from saturated until air-dry was 510 minutes for the quartz sand, 480 minutes for the masonry sand, and 1020 minutes for the Ithaca soil.

5.4 A simple model

The general pattern of the change in band depth with water content can be duplicated using a very simple model, illustrated in Figure 5.13. Consider reflectance from a slab of material, covered by a layer of water of depth, h. Radiance, L_d, illuminates the surface, undergoes reflection, R_w, at the water surface, and is refracted into the water at an angle, θ. The radiance propagates through the water, attenuated only by absorption, a. The light is then reflected from a planar surface with reflectance, R_{ws}, which we will assume to be spectrally flat over the range of the absorption band. The reflected light returns to the water surface, again undergoes reflection and refraction, and exits the water surface as radiance, L_u. The observed radiance, L_u, is given by,

$$L_u = L_d R_{ws}(1 - R_w)^2 e^{-2ah \sec\theta} \quad , \tag{5.1}$$

and the reflectance is then,

$$R = \frac{L_u}{L_d} = R_{ws}(1 - R_w)^2 e^{-2ah \sec\theta} \quad . \tag{5.2}$$

Since Fresnel reflectance, R_w, at the water surface is slowly varying spectrally it is treated as a constant with $R_w \approx 0.02$. For our purposes the angle of incidence will not affect the relative change, and we will consider normal incidence and viewing, $\theta = 0$. Finally, we ignore scattering losses, since over these short distances and at the wavelengths of interest, absorption will dominate the transmission loss. With these simplifying assumptions, the reflectance from the water-coated surface is given by:

$$R = \frac{L_u}{L_d} = k\, e^{-2ah} \quad , \tag{5.3}$$

where $k = R_{ws}(1 - R_w)^2$. Equation 5.3(5.3) describes the two transmissions at the air-water interface, $(1 - R_w)^2$, a reflection at the water-soil interface, R_{ws}, and the two-way transmission through the water, $e^{-2ah\sec\theta}$. The absorption band depth 4.2 can then be written,

$$\Delta R_c = R_{int} - R_c = k[e^{-2a_{int}h} - e^{-2a_c h}] \quad , \tag{5.4}$$

where $k = 0.96\, R_{ws}$, a_c is the water absorption coefficient at the center of the water absorption band, and a_{int} is the interpolated water absorption coefficient at the band center. The value used for R_{ws} was the reflectance observed from each sample at the point of the minimum slope (dashed line in Figure 5.9). At that point, the sample appeared dry visually, but the spectrum was noticeably altered, indicating that there was water at the surface. The model values for ΔR_c are shown in Figure 5.14 for the four absorption bands as the depth, h, varies.

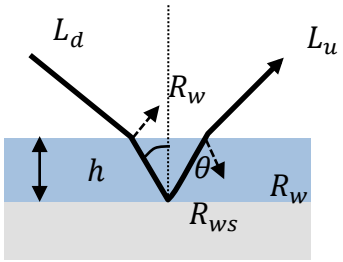

Figure 5.13: Illustration of a model of reflectance from a spectrally uniform, flat surface covered with a layer of water of depth, h.

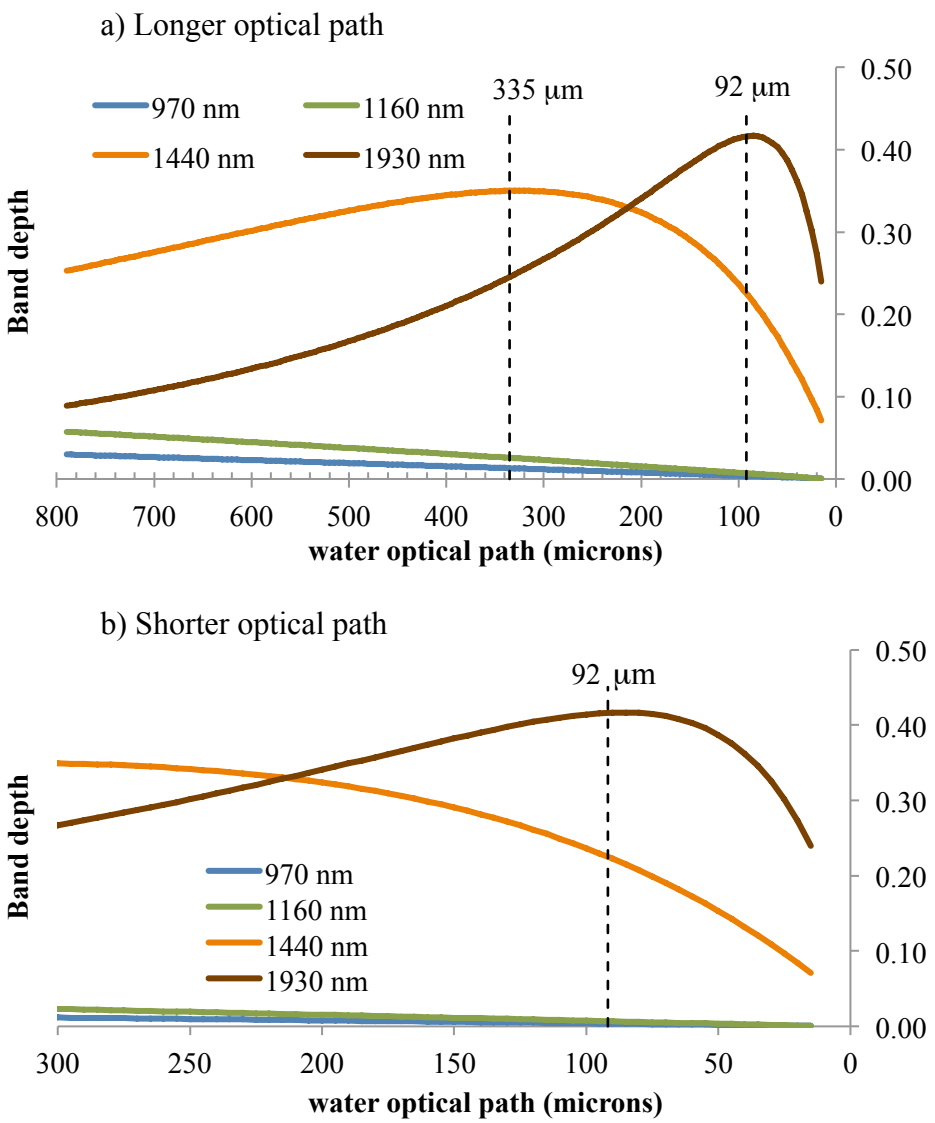

Figure 5.14: Modeled change in band depth vs. water optical path. a) exhibits a longer optical path range to simulate quartz sand in band depth shape, and b) exhibits a shorter optical path rage to simulate masonry sand and Ithaca soil in band depth shape. Dashed line (335 μm) marks the approximate break point between segment-A and segment-B for quartz sand and dashed line marks the approximate end of segment-B for all three soils.

This simple model reproduces the general shape of the curves in Figure 5.9. It also provides a basis for considering some of the general properties of the wet soil reflectance. Firstly, all four band depths are described by the same equation in which only the absorption coefficients and the reflectance at the water-soil interface change. The peak observed in the

1930 nm data late in the drying period is a function of the magnitude of the absorption coefficient over the wavelength range and the strength of the contrast between absorption at the center and shoulders of the band. Absorption at the band center, being about an order of magnitude greater than the absorption at the shoulders, dominates the change in band depth for very small h, but after most of the light at the center wavelength has been absorbed, i.e., as $e^{-a_c h} \longrightarrow 0$, further change is controlled by absorption at the shoulder wavelengths.

The maximum depth, h_{max}, can be found by taking the derivative of Equation (5.4, setting it equal to zero and solving for h,

$$h_{max} = \frac{ln(a_c/a_{int})}{2(a_c - a_{int})} \quad . \tag{5.5}$$

For the absorption feature at 1930 nm, the water absorption coefficient at the band center is $a_c = 136.7\ cm^{-1}$, and the interpolated absorption value is $a_{int} = 14.5\ cm^{-1}$, which yields an effective optical depth, $h_{max} = 91.8\ microns$. A similar peak is apparent in the band depth curve for 1440 nm. Its location is a function of the absorption coefficients in that wavelength range. The peak is shifted to an earlier time and corresponds to a greater optical path, with $h_{max} \approx 335\ microns$. The model predicts a peak for the band depth at 970 nm and 1160 nm band as well; however the absorption coefficients are low enough that light that is not absorbed would be reflected before the required optical path (on the order of a centimeter) is achieved.

This is a simplistic model which serves to demonstrate that there is a link between the observations of the changing band depth at different wavelengths and an effective optical path, h. However, an actual optical path in soil is not a depth, as portrayed in the model, but a segmented path that includes multiple reflections and refractions, and represents an average path of all the photons reaching the detector. Another important point is that this model is only

appropriate when the first contact of light is with water. When there is no longer a nearly continuous covering of adsorbed water, i.e., when dry particle surfaces start to appear, this model breaks down.

6. Conclusion

To study the relationship between soil spectral reflectance features and water content, three soil samples were chosen to represent a range of properties: particle size distribution, texture and drying characteristics, and significant differences in the general shape of the spectral reflectance of dry samples. In contrast to earlier studies which were restricted to occasional reflectance observations, reflectance was monitored at 5 minute intervals throughout the drying process, which was due entirely to evaporation, and changing weight of sample was collected to characterize the sample water content.

Working from the assumption that water absorption bands would be the spectral features most sensitive to subtle changes in water content, this work focused on the most prominent bands in the shortwave infrared, those centered at 970, 1160, 1440, and 1930 nm. Band depth was selected as the primary metric since that would be most likely to be independent of soil type, and would be most directly related to the water content. The band depth for the 970 nm and 1160 nm absorption bands were only apparent in the quartz sand sample, so the focus was on the water absorption features in SWIR region.

In graphs of the change in band depths with time, the changes appeared to group into relatively stable, nearly linear segments for all three soils. During the initial drying stage, the quartz sand data had two distinct segments while masonry sand and Ithaca soil had only one. After a short, non-linear transition period, the final two segments – a rapid decrease in band depth and a final slow steady decrease – were consistent for all three samples, although the duration for each segment varied among the different soils. Counterintuitively, the band depth for 1440 nm and 1930 nm did not decrease monotonically over time as the VWC decreased.

Even more interestingly, the 1930 nm band depth for each soil sample initially increased, reached a maximum value, and then decreased rapidly to a final stable level. The maximum band depth for each soil sample occurred at different VWC values, strongly suggesting that a relationship between band depth and VWC will not be independent of soil types.

Though the relationship between water absorption band depth and water content is not independent of soil type, the band depth is related to the evaporation process. For all three soils, the evaporation rate was essentially constant at first, and then decreased sharply, as has been observed in studies of evaporation from soil. For all three soil samples, the water absorption band depth centered at 1930 nm increased steadily while the evaporation was constant. In every case, the band depth decreased abruptly, coincident with the decrease in evaporation rate. These two features are both likely to be related to the loss of pore water and the initiation of the slower evaporation of adsorbed water.

As illustrated with a simple model, the band depth maximum resulted from the strong contrast in absorption coefficients at the center and shoulder wavelengths, with absorption at 1930 nm being strong enough that light at that wavelength was almost completely extinguished by absorption after traveling only a short optical path through the water. The optical path required to extinguish light at 1930 nm appears to match the very small amount of water available near the end of the drying period. As a result, the maximum band depth and the rapid decrease in band depth coincided with the transition from stage-1 to stage-2 drying. This occurred for all three soils even though the particle size (and pore size) distribution, drying time, and water content at the time of the transition varied greatly among the three soil samples.

Some specific conclusions are:

1. The water absorption bands at 970 nm and 1160 nm are less suitable for relating the estimation of soil water content, but their existence may help identify some types of soil, or some physical features of the soil.
2. The minimum sample depth required to avoid reflected light from the bottom of the sample holder is greater for saturated samples than for dry samples, and the influence of water content affected the white, relatively translucent sand more than the darker, more opaque samples. With water in pore spaces and coated on soil particles, more light is forward scattered and penetrates deeper into the soil.
3. For all three kinds of soils, during their drying process, a non-linear transition segment always occurs between a gently changing segment and an abruptly decreasing segment.
4. For white sand, both the 1440 nm and 1930 nm curves can be divided into four roughly linear segments. For the masonry sand and Ithaca soil, the 1440 nm band is divided into three segments, and the 1930 nm band is partitioned into four segments. The linear segments for the 1440 nm band are less noisy and generally provide a better model of the soil water content.
5. The break points of different kinds of soils in the drying process might be an indicator for soil properties. The VWC values of break points at the beginning of segment-C are 0.016, 0.064 and 0.188 (based on 1930 nm band segmentation), respectively for quartz sand, dark sand and Ithaca soil. The Ithaca soil is the finest soil, and the white sand has the largest particle size, so the break points might be result of soil particle effects.

Although the initial hypothesis – that the water absorption band depths would be independent of soil type and structure – failed, another relation between water absorption band

depth and evaporation rate was found. It remains to verify and expand on these results by examining a wider range of soil types under controlled conditions, and modeling the underlying processes.

Reference

Ahmad, A., Zhang, Y. & Nichols, S., 2011. Review and evaluation of remote sensing methods for soil-moisture estimation. *Journal of Photonics for Energy*, p.028001. Available at: http://photonicsforenergy.spiedigitallibrary.org/article.aspx?doi=10.1117/1.3534910.

Albergel, C. et al., 2008. From near-surface to root-zone soil moisture using an exponential filter: an assessment of the method based on in-situ observations and model simulations. *Hydrology and Earth System Sciences Discussions*, 5(3), pp.1603–1640. Available at: http://www.hydrol-earth-syst-sci-discuss.net/5/1603/2008/.

Baret, F., Jacquemoud, S. & Hanocq, J.F., 1993. The soil line concept in remote sensing. *Remote Sensing Reviews*, 7(1), pp.65–82. Available at: http://www.tandfonline.com/doi/abs/10.1080/02757259309532166.

Van Brakel, J. & Heertjes, P.M., 1978. On the period of constant drying rate. *Proceedings of the 1st Symposium on Drying*, pp.70–75.

Chang, C.-W., Laird, D.A. & Hurburgh, Ch.R., 2005. Influence of Soil Moisture on Near-Infrared Reflectance Spectroscopic Measurement of Soil Properties. *Soil Science*, 170(4), pp.244–255.

Choudhury, B.J. et al., 1979. Effect of surface roughness on the microwave emission from soils. *Journal of Geophysical Research*, 84(C9), p.5699. Available at: http://doi.wiley.com/10.1029/JC084iC09p05699.

Clark, R.N. & Roush, T.L., 1984. Reflectance spectroscopy: Quantitative analysis techniques for remote sensing applications. *Journal of Geophysical Research*, 89(B7), p.6329.

Ford, T.W., Harris, E. & Quiring, S.M., 2014. Estimating root zone soil moisture using near-surface observations from SMOS. *Hydrology and Earth System Sciences*, 18(1), pp.139–154. Available at: http://www.hydrol-earth-syst-sci.net/18/139/2014/.

Gaskin, G.J. & Miller, J.D., 1996. Measurement of Soil Water Content Using a Simplified Impedance Measuring Technique. *Journal of Agricultural Engineering Research*, 63(2), pp.153–159. Available at: http://www.sciencedirect.com/science/article/B6WH1-45NJM06-8/2/5f7746bddafa8011432f5778e3d7debb.

Jackson, J., 1982. Under Vegetation Canopies = Tv. *Water Resources*, 18(4), pp.1137–1142.

Jackson, T.J. & Schmugge, T.J., 1991. Vegetation effects on the microwave emission of soils. *Remote Sensing of Environment*, 36(3), pp.203–212. Available at: http://linkinghub.elsevier.com/retrieve/pii/003442579190057D.

Kaleita, a L., Tian, L.F. & Hirschi, M.C., 2005. Relationship between soil moisture content and soil surface reflectance. *Transactions of the Asae*, 48(5), pp.1979–1986. Available at: <Go to ISI>://000233151400035.

Kerr, Y.H. & Njoku, E.G., 1990. Semiempirical model for interpreting microwave emission from semiarid land surfaces as seen from space. *IEEE Transactions on Geoscience and Remote Sensing*, 28(3), pp.384–393.

Kou, L., Labrie, D. & Chylek, P., 1993. Refractive indices of water and ice in the 065- to 25-μm spectral range. *Applied Optics*, 32(19), p.3531.

Lehmann, P. & Or, D., 2009. Evaporation and capillary coupling across vertical textural contrasts in porous media. *Physical Review E*, 80(4), p.46318.

Lesaignoux, A. et al., 2010. Estimation of Soil Moisture Content of bare soils from their spectral optical properties in the 0.4 - 12 μm spectral domain. In *2010 IEEE International Geoscience and Remote Sensing Symposium*. IEEE, pp. 3861–3864. Available at: http://ieeexplore.ieee.org/lpdocs/epic03/wrapper.htm?arnumber=5649907.

Lesaignoux, A., Fabre, S. & Briottet, X., 2013. Influence of soil moisture content on spectral reflectance of bare soils in the 0.4–14 μm domain. *International Journal of Remote Sensing*, 34(7), pp.2268–2285.

Liang, S., 1997. An investigation of remotely-sensed soil depth in the optical region. *Int. J. Remote Sensing*, 18(16), pp.3395–3408.

Liu, W. et al., 2002. Relating soil surface moisture to reflectance. *Remote Sensing of Environment*, 81(2–3), pp.238–246.

Lobell, D.B. & Asner, G.P., 2002. Moisture effects on soil reflectance. *Soil Science Society of America Journal*, 66(3), pp.722–727.

Mahfouf, J.-F., 1991. Analysis of Soil Moisture from Near-Surface Parameters: A Feasibility Study. *Journal of Applied Meteorology*, 30(11), pp.1534–1547. Available at: http://journals.ametsoc.org/doi/abs/10.1175/1520-0450%281991%29030%3C1534%3AAOSMFN%3E2.0.CO%3B2 [Accessed July 30, 2015].

Mo, T., Schmugge, T. & Wang, J., 1987. Calculations of the microwave brightness temperature of rough soil surfaces: bare field. *Geoscience and Remote ...*, GE-25(1), pp.47–54. Available at: http://ieeexplore.ieee.org/lpdocs/epic03/wrapper.htm?arnumber=4072598\nhttp://ieeexplore.ieee.org/xpls/abs_all.jsp?arnumber=4072598.

Neema, D.L., Shah, A. & Patel, a. N., 1987. A statistical optical model for light reflection and

penetration through sand. *International Journal of Remote Sensing*, 8(8), pp.1209–1217. Available at: http://www.tandfonline.com/doi/abs/10.1080/01431168708954765.

Njoku, E.G. & Entekhabi, D., 1996. Passive microwave remote sensing of soil moisture. *Journal of Hydrology*, 184(1-2), pp.101–129. Available at: http://www.sciencedirect.com/science/article/pii/0022169495029702 [Accessed April 3, 2015].

Njoku, E.G. & Rague, B.W., 1996. Spatial and temporal trends in land surface moisture and temperature observable using data from the nimbus-7 microwave radiometer. In *IGARSS 96 Remote Sensing for a Sustainable Future*. CALTECH, JET PROP LAB,PASADENA,CA 91109.: IEEE, p. 1057.

Oki, T. & Kanae, S., 2006. Global Hydrological Cycles and World Water Resources. *Science*, 313(5790, Freshwater Resources), pp.1068–1072.

Or, D. et al., 2013. Advances in Soil Evaporation Physics—A Review. *Vadose Zone Journal*, 12(4). Available at: https://www.soils.org/publications/vzj/pdfs/12/4/vzj2012.0163?search-result=1 [Accessed July 3, 2015].

Ozcep, F., Tezel, O. & Asci, M., 2009. Correlation between electrical resistivity and soil-water content: Istanbul and Golcuk. *International Journal of Physical Sciences*, 4(6), pp.362–365. Available at: http://www.academicjournals.org/journal/IJPS/article-abstract/83DBF6019062 [Accessed July 30, 2015].

Pampaloni, P. & Paloscia, S., 1986. Microwave Emission and Plant Water Content: A Comparison between Field Measurements and Theory. *IEEE Transactions on Geoscience and Remote Sensing*, GE-24(6), pp.900–905.

Parent, A.-C., Anctil, F. & Parent, L.-É., 2006. Characterization of temporal variability in near-surface soil moisture at scales from 1 h to 2 weeks. *Journal of Hydrology*, 325(1–4), pp.56–66.

Planet, W.G., 1970. Some comments on reflectance measurements of wet soils. *Remote Sensing of Environment*, 1(2), pp.127–129.

Sabater, J.M. et al., 2007. From Near-Surface to Root-Zone Soil Moisture Using Different Assimilation Techniques. *Journal of Hydrometeorology*, 8(2), pp.194–206. Available at: http://journals.ametsoc.org/doi/abs/10.1175/JHM571.1.

Sadeghi, M., Jones, S.B. & Philpot, W.D., 2015. A linear physically-based model for remote sensing of soil moisture using short wave infrared bands. *Remote Sensing of Environment*, 164(0), pp.66–76.

Stoner, E.R. & Baumgardner, M.F., 1981. Characteristic Variations in Reflectance of Surface

Soils1. *Soil Science Society of America Journal*, 45(6), p.1161. Available at: https://www.soils.org/publications/sssaj/abstracts/45/6/SS0450061161.

Tsang, L. & Newton, R.W., 1982. Microwave emissions from soils with rough surfaces. , 87(11), pp.9017–9024.

Tsang, L., Njoku, E. & Kong, J. a., 1975. Microwave thermal emission from a stratified medium with nonuniform temperature distribution. *Journal of Applied Physics*, 46(12), p.5127. Available at: http://scitation.aip.org/content/aip/journal/jap/46/12/10.1063/1.321571.

Wagner, W. et al., 2006. Operational readiness of microwave remote sensing of soil moisture for hydrologic applications.

Walker, J.P., Willgoose, G.R. & Kalma, J.D., 2001. One-dimensional soil moisture profile retrieval by assimilation of near-surface observations: a comparison of retrieval algorithms. *Advances in Water Resources*, 24(6), pp.631–650. Available at: http://linkinghub.elsevier.com/retrieve/pii/S0309170800000439.

Wigneron, J.P. et al., 1998. Use of passive microwave remote sensing to monitor soil moisture. *Agronomie*, 18(1), pp.27–43.

Wilheit, T.T., 1978. Radiative Transfer in a Plane Stratified Dielectric. *IEEE Transactions on Geoscience Electronics*, 16(2), pp.138–143.

Yiotis, A.G. et al., 2006. Pore-network study of the characteristic periods in the drying of porous materials. *Journal of colloid and interface science*, 297(2), pp.738–748. Available at: http://www.sciencedirect.com/science/article/pii/S0021979705012208.

Zhu, Y. et al., 2010. Characterizing surface soil water with field portable diffuse reflectance spectroscopy. *Journal of Hydrology*, 391(1-2), pp.133–140. Available at: http://www.sciencedirect.com/science/article/pii/S0022169410004397 [Accessed July 30, 2015].